Listeria monocytogenes InlP interacts with afadin and facilitates basement membrane crossing

Cristina Faralla[a,b,i] *, Effie E. Bastounis[c] *, Fabian E. Ortega[c] , Samuel H. Light[d], Gabrielle Rizzuto[a,b] , Salvatorre Nocadello[d], Wayne F. Anderson[d], Jennifer R. Robbins[e], Julie A. Theriot[c,f,g], and Anna I. Bakardjiev[a,b,h]

*These authors contributed equally

[a] Benioff Children's Hospital, University of California, San Francisco, San Francisco, California;

[b]Program in Microbial Pathogenesis and Host Defense, University of California, San Francisco, San Francisco, California;

[c]Department of Biochemistry, Stanford University School of Medicine, Stanford, California;

[d]Center for Structural Genomics of Infectious Diseases and Department of Biochemistry and Molecular Genetics, Feinberg School of Medicine, Northwestern University, Chicago, Illinois;

[e]Department of Biology, Xavier University, Cincinnati, Ohio;

[f]Department of Microbiology and Immunology, Stanford University School of Medicine, Stanford, California;

[g]Howard Hughes Medical Institute, Stanford University School of Medicine, Stanford, California;

[h]Current address: VIR Biotechnology, San Francisco, California

[i]Current address: AbCellera Biologics Inc., Vancouver, BC, Canada

Corresponding author: abakardjiev@vir.bio

24 Short title: *L. monocytogenes* InlP binds afadin

25

ABSTRACT

During pregnancy, the placenta protects the fetus against the maternal immune response, as well as bacterial and viral pathogens. Bacterial pathogens that have evolved specific mechanisms of breaching this barrier, such as *Listeria monocytogenes*, present a unique opportunity for learning how the placenta carries out its protective function. We previously identified the *L. monocytogenes* protein Internalin P (InlP) as a secreted virulence factor critical for placental infection (1). Here, we show that InlP, but not the highly similar *L. monocytogenes* internalin Lmo2027, binds to human afadin (encoded by *AF-6*), a protein associated with cell-cell junctions. A crystal structure of InlP reveals several unique features, including an extended leucine-rich repeat (LRR) domain with a distinctive Ca^{2+}-binding site. Despite afadin's involvement in the formation of cell-cell junctions, MDCK epithelial cells expressing InlP displayed a decrease in the magnitude of the traction stresses they could exert on deformable substrates, similar to the decrease in traction exhibited by *AF-6* knock-out MDCK cells. *L. monocytogenes ΔinlP* mutants were deficient in their ability to form actin-rich protrusions from the basal face of polarized epithelial monolayers, a necessary step in the crossing of such monolayers (transcytosis). A similar phenotype was observed for bacteria expressing an internal in-frame deletion in *inlP* (*inlP* ΔLRR5) that specifically disrupts its interaction with afadin. However, afadin deletion in the host cells did not rescue the transcytosis defect. We conclude that secreted InlP targets cytosolic afadin to specifically promote *L. monocytogenes* transcytosis across the basal face of epithelial monolayers, which may contribute to the crossing of the basement membrane during placental infection.

47 **INTRODUCTION**

48 During pregnancy, the consequences of placental infection can be severe, ranging from
49 maternal sepsis to miscarriage, and can lead to pre-term birth and lifelong disability (2).
50 Fortunately, such infections are relatively rare – which stands as a testament to the strength of the
51 feto-maternal barrier. Despite serving such an important function, the molecular, cellular and
52 histological components of feto-maternal barrier have only just begun to be elucidated. Because
53 the barrier is so effective at preventing infection, pathogens that do manage to cross it must have
54 evolved strategies of countering host defenses and thus provide a unique opportunity for
55 addressing the mechanistic features that make the feto-maternal barrier so formidable (3).
56 *Listeria monocytogenes* is a well-characterized food-borne pathogen capable of
57 placental crossing and is thus ideal for probing this barrier (4). In the healthy, non-pregnant adult,
58 it causes gastrointestinal illness, but in immunocompromised individuals meningitis can result,
59 and in pregnant women, sepsis, spontaneous abortion, preterm labor, infant brain damage and
60 death are possible outcomes (5). After ingestion, *L. monocytogenes* infects epithelial cells of the
61 intestine, mainly via interactions between the bacterial surface protein Internalin (encoded by the
62 gene *inlA*) and the host cell receptor E-cadherin, which is exposed at the tips of intestinal villi (6-
63 8). After uptake by an intestinal epithelial cell, the bacterium escapes the resulting phagosome and
64 replicates in the host cytoplasm, where it induces actin polymerization, forming actin comet tails
65 that drive its rapid motility (9). Upon reaching the host plasma membrane, *L. monocytogenes* can
66 form a membrane-bound protrusion that pushes its way into a neighboring cell. Engulfment of the
67 protrusion by the neighboring cell leaves the bacterium in a double-membrane vacuole from
68 which it escapes, resetting its life cycle (9, 10). From the initial site of infection in the intestinal
69 epithelium, *L. monocytogenes* can spread via actin-based motility into immune cells, which

70 facilitate spread throughout the host while protecting the pathogen from humoral immune
71 defenses (11, 12). Actin-based cell-to-cell spread is thought to contribute to the ability of *L.*
72 *monocytogenes* to evade the host immune system and to penetrate a variety of protective barriers
73 in the host (13), including the blood-brain barrier and the feto-maternal barrier in the placenta (14-
74 16).

75 A clue to the protective nature of the feto-maternal barrier lies in the fact that almost all
76 pathogens that cross it are known to have an intracellular aspect to their life cycle—they move
77 *through* cells from mother to fetus (3). Two interfaces are available; each is unlike any other part
78 of the mammalian body. The first, where fetal extravillous trophoblasts (EVTs) anchor the
79 placenta in uterine decidua, has a unique immune environment (17). The trophoblasts possess
80 innate immune defense properties shown to prevent bacterial infection (18) and restrict growth of
81 intracellular *L. monocytogenes* (19). The second, much more extensive interface is composed of
82 fetal syncytiotrophoblasts (STB) which form a vast, thin multinucleate layer without cell-cell
83 junctions, bathed in maternal blood. This is the site of gas and nutrient/waste exchange.
84 Underlying the STB is a second, single-celled layer of individual, self-renewing cytotrophoblasts
85 (CTBs) that periodically fuse with the STB to allow its growth. Our previous work has shown that
86 the STB's lack of cell-cell junctions (20) and the syncytial stiffness generated by dense networks
87 of actin filaments (21) act as significant deterrents to STB infection by pathogens. Rather,
88 infection of human placental organ cultures suggests that the first interface, where EVTs contact
89 uterine decidua, is the preferred route of placental infection by *L. monocytogenes*, which then
90 spreads via actin-dependent cell-to-cell spread to the CTB monolayer underlying the STB (20).
91 But even once *L. monocytogenes* has reached the subsyncytial CTBs, most bacterial movement

92 occurs laterally from cell to cell within the monolayer, and it only rarely transcytoses in a
93 direction perpendicular to the monolayer to colonize the fetal stroma beneath it (20).
94 Recently, we used an unbiased genetic screen in a pregnant guinea pig model of listeriosis
95 to identify *L. monocytogenes* genes that contribute specifically to infection of the placenta. (1).
96 One gene identified in this screen encodes InlP, a member of the internalin family of proteins.
97 Pathogenic *L. monocytogenes* contain genes for 25 known members of this protein family, which
98 share a common overall structure that includes a secretory signal sequence at the N terminus and a
99 large leucine-rich repeat domain, a motif frequently implicated in protein-protein interactions
100 (22). The two best-characterized internalins, InlA and InlB, contribute to *L. monocytogenes*
101 invasion of epithelial cells and hepatocytes by binding to their cognate host cell surface receptors,
102 E-cadherin and c-Met respectively (6, 23). While most internalins are predicted to be anchored to
103 the bacterial cell surface via attachment to the peptidoglycan cell wall or to lipoteichoic acids,
104 four of them, including InlP, lack obvious anchoring domains and are predicted to be secreted by
105 the bacterium (24). In order to address the mechanism by which InlP assists *L. monocytogenes* in
106 crossing the feto-maternal barrier, we set out to find host protein binding partners. In this work,
107 we identify the host cell cytoplasmic protein afadin as a major binding partner for InlP, and
108 demonstrate that the InlP-afadin interaction specifically enhances *L. monocytogenes*
109 transcytosis—that is, the ability of *L. monocytogenes* to exit from the basal face of an infected
110 polarized epithelial monolayer, consistent with its potential contribution to placental infection.

111 **MATERIALS AND METHODS**

112 **Study approval.** Human subjects: This study was conducted according to the principles
113 expressed in the Declaration of Helsinki. The study was approved by the Institutional Review
114 Board at the University of California, San Francisco, where all experiments were performed
115 (CHR# 11-05530). All patients provided written informed consent for the collection of samples
116 and subsequent analysis.

117 **Recombinant InlP expression and purification.** All chemicals were purchased from
118 Sigma-Aldrich unless otherwise stated. Center for the Structural Genomics of Infectious Diseases
119 (CSGID) standard protocols were used for cloning, over-expression, and purification of InlP (25,
120 26). Briefly, InlP (from residue 31-388) and Lmo2027 (from residue 31-367) were cloned into the
121 pMCSG7 expression vector (http://bioinformatics.anl.gov/mcsg/technologies/vectors.html).
122 Following transformation into the BL21 (DE3) Magic *E. coli* strain, cells were grown in
123 M9-selenomethionine medium or Terrific Broth (TB) at 37 °C up to an OD_{600} of 1. At that point,
124 the temperature was reduced to 25 °C and protein over-expression was induced by the addition of
125 isopropyl-1-thio-D-galactopyranoside (IPTG) to a final concentration of 1 mM. After 16 h, cells
126 were harvested by centrifugation, suspended in a buffer containing 10 mM Tris-HCl pH 8.3, 500
127 mM NaCl, 10% glycerol, and 1 mM Tris (2-carboxyethyl) phosphine hydrochloride (TCEP) and
128 lysed by sonication. InlP was purified by Ni-NTA affinity chromatography and eluted with a
129 buffer containing 10 mM Tris-HCl pH 8.3, 500 mM NaCl, 1 mM TCEP. The His-tag was cleaved
130 overnight at 4°C incubating the enzymes with His-tagged TEV protease. The protein samples
131 were then reloaded onto the nickel column and the flow-through was collected. At this point, the
132 protein was concentrated using Vivaspin centrifugal concentrators (GE Healthcare Life Sciences)

133 and both its size and purity were checked by SDS-PAGE.

134

135 **InlP and Lmo2027 structure determination.** Sitting drop crystallization plates were set
136 up at room temperature. InlP crystals were obtained with a 1:1 mixture of 8.5 mg/mL InlP in 10
137 mM Tris pH 8.3, 1 mM TCEP and condition D11 from the Qiagen PACT crystallization screen
138 (0.2 M Calcium chloride, 0.1 M Tris pH 8, 20% (w/v) PEG 6000). Lmo2027 crystals were
139 obtained with a 1:1 mixture of 12.6 mg/mL Lmo2027 and 10 mM Tris pH 8.3, 0.5 M NaCl, and 1
140 mM TCEP and condition D4 from the Qiagen Classics II crystallization screen (0.1 M Citric acid
141 (pH 3.5) and 20% (w/v) PEG 3350). Harvested crystals were transferred to the mother liquor
142 before being frozen in liquid nitrogen. Diffraction data were collected at 100° K at the Life
143 Sciences Collaborative Access Team at the Advance Photon Source, Argonne, Illinois (APS
144 BEAMLINE 21-ID-G). All structural work was performed by the CSGID (25). Data were
145 processed using HKL-2000 for indexing, integration, and scaling (27). A selenomethionine
146 derivative of InlP was used to phase the structure by single-wavelength anomalous diffraction.
147 Lmo2027 was phased by molecular replacement, using the InlP structure as a starting model.
148 Structure was refined with Refmac (28). Models were displayed in Coot and manually corrected
149 based on electron density maps (29). All structure figures were prepared using PyMOL Molecular
150 Graphics System, Version 1.3 (Schrödinger, LLC).

151

152 **Isothermal titration calorimetry (ITC).** For ITC experiments, InlP was prepared by
153 overnight dialysis in ITC buffer (50 mM HEPES pH 7.5 and 150 mM NaCl). Experiments were
154 performed on the MicroCal ITC200 instrument (GE Healthcare). InlP was loaded into the cell at
155 0.12 mM and 25° C. Calcium chloride titrant (3.13 mM) dissolved in leftover dialysis buffer was

156 loaded into the syringe. Syringe rotation was set at 1000 RPM, with titrant injections spaced at
157 2 min intervals. The initial 0.2 µL injection was excluded from the data and the nineteen
158 subsequent 2.0 µL injections were used for data analysis. Binding parameters were obtained by
159 fitting isotherms using the Origin 7 (OriginLab, Northampton, MA) software package.
160
161 **Yeast two-hybrid, mass spectrometry analysis and pull-down assay.** Yeast two-hybrid
162 analysis was performed by Hybrigenics (France). Briefly, InlP (aa 31-388) was used to screen a
163 human placenta cDNA library. Clones expressing proteins with positive interactions with InlP
164 were isolated and sequenced.
165 For the GST-pull down experiments bait proteins were prepared as follows: Cloning: *inlP*
166 gene (from residue 31-388, oligo Fw2470 EcoRI-pGex CCGAATTCC
167 GCTTCTGATTTATATCCACTACCT, Rv2470 XhoI-pGex aGCTCGAG
168 TCATTAATAGTTACATTCCAATCATAAGAG) or Lmo2027 (from residue 31-367, oligo
169 Fw2027 EcoRI-pGex CCCCGAATTCCGCATCCGATTTATATCCACT ACC, Rv2027 XhoI-
170 pGex GAAGCTCGAGCTACTAATTAACCGTAAGTACCC) were cloned in pGEX-4T vector
171 (GE Healthcare) using restriction enzymes following transformation in BL21 DE3 *E. coli* strain.
172 InlPΔLRR5, InlPΔLRR7 and InlPΔLRR8, lacking the LRR5 (Δamino acids 174-195), the LRR7
173 motifs (Δamino acids 218-239) and the LRR8 (Δamino acids 240-261) respectively were
174 generated using Site Directed Mutagenesis (SDM) on the *inlP*-pGEX-4T vector following In-
175 Fusion® HD Cloning Kit protocol (Takara Bio USA, Inc.) using the following primers : ΔLRR5-
176 fw:GATTTCACTGGAATGCCTATTCCTTTACTTATTACGTTGGATCTAAG, ΔLRR5-rv:
177 CGTAATAAGTAAAGGAATAGG CATTCCAGTGAAATCAGGGATAGA; ΔLRR7-fw
178 CCTGATTTTCAAAATTTACCT AAATTAACTGATTTAAATTTAAGAC, ΔLRR7-rv:

179 AGTTAATTTAGGTAAATTTTGAAAATCAGGAATAGTTGTCA, ΔLRR8-fw:
180 CCTGATTTTCAAA ATAACTTACCTAGTTTAGAATCCTTAAACT ΔLRR8-rv:
181 TAAACTAGGTAAGTTATTTTGAAAATCAGGTGTATTGGTTAA. Baits purification: BL21
182 DE3 *E. coli* carrying pGEX-4T, pGEX-4T-*2027,* pGEX-4T-*inlP,* pGEX-4T-*inlP*Δ*LRR5,* pGEX-
183 4T-*inlP*Δ*LRR7* or pGEX-4T-*inlP*Δ*LRR8,* were grown until OD 0.6 in 250 mL of LB
184 supplemented with 100 µg/mL ampicillin at 37 °C and 180 rpm. GST or GST-
185 InlP/2027/ΔLRR5/ΔLLR7/ΔLRR8 expression were then induced with 0.2 mM IPTG for 4 h at
186 30 °C 180 rpm. Pellet from 250 mL of culture was lysed with 35 mL of cell lytic express (Sigma)
187 and the soluble fraction was incubated overnight with 5 mL of Glutathione Sepharose™ 4B (GE
188 Healthcare) under constant agitation. GST-Glutathione Sepharose™ 4B or GST-
189 InlP/2027/ΔLRR5/ΔLLR7/ΔLRR8/ - Glutathione Sepharose™ 4B were then collected and washed
190 with 100 mL of PBS at 500 x g and stored at 4 °C in Tris-HCl 50 mM, NaCl 50 mM pH 8.
191 For preparation of protein extracts for pull-down experiments with human placenta: 2.3
192 grams of placental villi (~21 weeks gestational age) were lysed in 10 mL of M-PER™ (Thermo
193 Fisher Scientific) supplemented with one tablet of complete Protease Inhibitor Cocktail (Roche)
194 and PhosSTOP phosphatase inhibitor (Roche). The sample was homogenized for 30 sec, sonicated
195 for 4 min and incubated for 1 h on ice. The soluble fraction was collected after centrifugation
196 14000 x g for 20 min at 4 °C, split in two and incubated overnight under constant agitation with 1
197 mL of GST-Glutathione Sepharose™ 4B, GST-InlP- Glutathione Sepharose™ 4B or GST-2027-
198 Glutathione Sepharose™ 4B respectively (prepared previously). The next day, washes were
199 performed with 50 mL PBS and elution fractions were collected with 3 mL Tris-HCl 50 mM,
200 NaCl 50 mM free glutathione 10 mM, pH 8. Elution fractions were run on 10% gel (NuPAGE™
201 Novex™ 10% Bis-Tris Protein Gels) and analyzed by Western blot, Coomassie blue staining

202 (SimplyBlue™ SafeStain, Life Technologies) or sent to Taplin Mass Spectrometry Facility at
203 Harvard Medical school for protein identification from SDS-PAGE gel (Supplementary Table 2).
204 In preparation of protein extracts for pull-down experiments with MDCK cells: one 75 mm
205 flask of MDCK or MDCK *AF-6*$^{-/-}$ cells polarized for three days was lysed in 180 µL of cell lytic M
206 supplemented with complete Protease Inhibitor Cocktail (Roche). The soluble fraction was split in
207 two and incubated overnight under constant agitation with 20 µL of GST-Glutathione Sepharose™
208 4B or GST-InlP/2027/ΔLRR5/ΔLRR7/- Glutathione Sepharose™ 4B respectively (prepared
209 previously). The day after beads were washed with 2 mL of Tris-HCl 50 mM, NaCl 50 mM, free
210 glutathione 10 mM, pH 8.0. The bound proteins were eluted by boiling the beads in SDS sample
211 buffer (NuPAGE® sample reducing agent 10X and NuPAGE® LDS sample buffer 4X) for 30
212 min and analyzed by Western Blot or Coomassie blue staining (SimplyBlue™ SafeStain, Life
213 Technologies) or sent to Taplin Mass Spectrometry Facility at Harvard Medical school for protein
214 identification (Supplementary Table 2 and Fig. 3D). Raw mass spectrometry data were then
215 further analyzed to determine differences in binding of proteins to InlP-GST versus InlPΔLRR5-
216 GST. First proteins identified by only 1 peptide in 1 or 2 samples were excluded from further
217 analysis. Then proteins found to bind to GST alone were also excluded from further analysis.
218 Finally proteins that showed 0 intensity for either InlP-GST or InlPΔLRR5-GST were also
219 excluded from the analysis. The resultant data and analysis are depicted in Fig. 3D and Fig. S4.
220 To detect afadin by Western Blot analysis, elution fractions were analyzed on 4-12% gels
221 (NuPAGE™ Novex™ 4-12% Bis-Tris Protein Gels) run on ice in MOPS buffer (NuPAGE®
222 MOPS SDS Running Buffer) for 3 h at 200 V and transfer was performed at 100V for 2 h.
223 Primary staining using mouse anti-afadin antibody (BD Transduction Laboratories™ , 1:2000) and
224 mouse anti- β-actin antibody (SIGMA, 1:1000) were incubated overnight at 4 °C. Secondary

225 antibody goat anti-mouse IgG-HRP (1:10000, Santa Cruz Biotechnology's) was incubated for 1 h
226 at room temperature. Protein detection was performed using ECL Western Blotting Substrate™
227 (Pierce).
228
229 **Human tissue collection and immunofluorescence.** For human placental organ cultures,
230 placentas from elective terminations of pregnancy (gestational age 4 to 8 weeks) were collected
231 and prepared as previously described (30). Briefly, fragments from the surface of the placenta
232 were dissected into 3-6 mm tree-like villi, placed on Matrigel (BD Biosciences)-coated Transwell
233 filters (Millipore, 30-mm diameter, 0.4 μm pore size) and cultured in Dulbecco's modified Eagle-
234 F12 medium (DMEM-F12; 1:1, vol/vol) supplemented with 20% FBS, 1% L-glutamine and 1%
235 penicillin/streptomycin (Invitrogen). Organ cultures were fixed for 15-30 min in 4%
236 paraformaldehyde at room temperature, flash frozen in Tissue-Tek O.C.T. Compound (Sakura
237 Finetek, Torrance, CA). Sections were cut at 7 μM, permeabilized for 5 min in ice-cold acetone,
238 dried, rehydrated in PBS, and blocked with Background Buster (Innovex Biosciences, Richmond,
239 CA). Primary staining with mouse anti-afadin antibody (BD Transduction Laboratories™ , 1:2000)
240 was incubated for 2 h at room temperature in PBS with 1% BSA and 5% normal goat serum
241 (Jackson ImmunoResearch Laboratories). Secondary staining with Alexa-Fluor® 594 goat anti-
242 mouse (1:500, ThermoFisher Scientific) was incubated for 1 h at room temperature, nuclei stained
243 with DAPI (Affymetrix), and sections mounted in Vectashield Mounting Medium (Vector
244 Laboratories). Stitched high-power images were acquired on a Nikon Ti-E epifluorescent
245 microscope with DS-Ri2 camera and NIS-Elements 4.30 software (Nikon Corporation).
246

247 **Mammalian cell line tissue culture.** MDCK (Madin Darby Canine kidney cell line,
248 ATCC), MDCK-AF6$^{-/-}$ (a generous gift from Denise Marciano, UT Southwestern) cells were
249 grown in Eagle's MEM (Minimal Essential Medium) with Earle's Balanced Salt Solution (BSS)
250 supplemented with 10% FBS. Invasion assays and growth curves were performed as previously
251 described (31). MDCK cells expressing a humanized version of InlP were generated as follows:
252 the IRES-GFP sequence was amplified from the pIRES-EGFP-puro plasmid (Addgene) using
253 oligo fw-IRESGFP-EcoRI: GGAATTCGAATTCTAAGCCCCTCTCCCTCCCCCC and rv-
254 IRESGFP-BamHI GGAATTCGGATCCTTACTTGTACAGCTC GTCCATGCCG and cloned
255 into the plasmid PCR2.1. The *inlP* gene was codon optimized for expression in mammalian cells
256 (h*inlP*) and the NheI-h*inlP*-Flag-EcoRI construct was synthesized by GeneWiz. Using the
257 restriction enzymes NheI and EcoRI the NheI-h*inlP*-Flag-EcoRI construct was then cloned into
258 PCR2.1-IRES-GFP. The construct NheI-h*inlP*-Flag-EcoRI-IRES-GFP-BamHI was then cut from
259 PCR2.1 using the restriction enzymes NheI-BamHI and cloned in pCW-Cas9-Blast (Addgene)
260 plasmid by replacing the Cas9 gene and generating the plasmid pCW- h*inlP*-Flag-IRES-GFP.
261 UCSF ViraCore (http://viracore.ucsf.edu/) was used to generate a Lentivirus strain carrying pCW-
262 h*inlP*-Flag-IRES-GFP, which was used to transduce MDCK or MDCK *AF-6*$^{-/-}$ cells. Viral
263 transduction was performed in 12-well plates as follows: freshly plated MDCK cells were allowed
264 to adhere for 1 h at 37 °C ($4x10^4$ cells/well), next nearly all media was removed and 350 µl of viral
265 supernatant was added to each well, followed by overnight incubation at 37 °C. The next morning
266 1 mL fresh media was added to each well without removing the viral supernatant and cells were
267 grown for 48-72 h, followed by puromycin selection (5 µg/mL) for another 4 days. Protein
268 expression was analyzed by Western Blot +/- addition of doxycycline 1 µg/mL. Primary staining:
269 mouse anti-flag antibody (1:5000), and mouse anti-β-actin antibody (SIGMA, 1:1000), secondary

270 antibody: goat anti-mouse IgG-HRP (1:10000, Santa Cruz Biotechnology). Protein detection was
271 performed using ECL Western Blotting Substrate™ (Pierce).
272
273 **Traction force microscopy (TFM).** Single cell TFM assays were performed as previously
274 described (32, 33). Two layered polyacrylamide hydrogels, the upper of which contained 0.04%
275 carboxylate-modified red latex beads of 0.1 μm in diameter (FluoSpheres; Molecular Probes)
276 were prepared and activated via SulfoSanpah crosslinker (Thermo Fischer Scientific, 22589) as
277 previously described (32, 33). Hydrogels were attached to 24-well glass bottom plates (MatTek)
278 to enable monitoring of multiple conditions simultaneously. The stiffness of the hydrogels was
279 5 kPa, achieved with a 5% final concentration of acrylamide (Sigma, A4058) and 0.15% final
280 concentration of bis-acrylamide (Fisher, BP1404-250). Activated hydrogels were coated with
281 collagen I (Sigma-Aldrich, C3867) overnight at 4 °C. Hydrogels were washed with PBS the next
282 day and equilibrated with cell media for 30 min at 37 °C prior to addition of cells.
283 For single cell TFM experiments, 2 mL containing $10x10^5$ cells were added on six-well TC
284 polystyrene plates for 24 h. Upon seeding 1 μg/mL doxycycline was added to the wells where InlP
285 expression was desired. The next day, cells were lifted via 0.25% trypsin-EDTA, washed once in
286 PBS and then cell pellets were re-suspended in media and $0.5x10^4$ cells in 1 mL were added per
287 hydrogel to achieve single cell attachment. Cells were allowed to adhere for 3 h at 37 °C before
288 imaging. To measure cell-ECM traction forces in confluent monolayers cells were added to a
289 concentration of $4x10^5$ cells per well directly onto the hydrogels 24 h prior to imaging. Upon
290 seeding 1 μg/mL doxycycline was added to the wells where InlP expression was desired.
291 Multi-channel time-lapse sequences of fluorescence (to image the beads within the upper
292 portion of the hydrogels) and phase contrast images (to image the cells) were acquired using an

293 inverted Nikon Diaphot 200 with a CCD camera (Andor Technologies) using a 40X Plan Fluor
294 NA 0.60 objective and the MicroManager software package (Open Imaging). In addition, at the
295 beginning and end of the recordings an image of the cells' nuclei stained with 1 μg/mL Hoechst
296 and an image of InlP fluorescence were acquired to ensure similar cell densities and similar InlP
297 expression across conditions, respectively. The microscope was surrounded by a cage incubator
298 (Haison) maintained at 37 °C and 5% CO_2. Images were acquired every 5 min for approximately 4
299 h. Subsequently, at each time interval we measured the 2D deformation of the substrate at each
300 point using an image correlation technique similar to particle image velocimetry (34). We
301 calculated the local deformation vector by performing image correlation between each image and
302 an undeformed reference image which we acquired by adding 10% SDS at the end of each
303 recording to detach the cells from the hydrogels. We used interrogation windows of 32 x 16 pixels
304 (window size x window overlap) for cells forming a monolayer or 32 x 8 pixels for single cells.
305 For single cell experiments, we used a custom algorithm using MATLAB (MathWorks) to
306 identify the contour of the cells from the phase contrast images (35). We calculated the two-
307 dimensional traction stresses that single cells exert to the hydrogel as described elsewhere (35).
308 We calculated the strain energy (U_s) as the mechanical work imparted by the cell to deform its
309 hydrogel:
310 $U_s = \frac{1}{2}\int_s \vec{\tau}(z=h)\cdot\vec{u}(z=h)\,ds$, where $\vec{u}$ is the measured displacement vector field on the free
311 surface of the hydrogel and $\int_s ()\,ds$ represents a surface integral. For cell monolayer experiments,
312 traction stresses were measured as described above and elsewhere (33, 36).
313
314 ***In vitro* transcytosis and invasion assays.** To quantify *L. monocytogenes* transcytosis,
315 MDCK cells were seeded on Transwell™ inserts with a 3-μm pore size loaded onto tissue culture-

316 treated 12-well plates (Corning, 3402) at a density of $5x10^5$ cells per insert three days prior to
317 infection. The day before infection, *L. monocytogenes* cultures were inoculated in 3 mL of Brain
318 Heart Infusion (BHI) directly from glycerol stocks and grown at 30 °C for 15 to 16 h without
319 agitation. The day of the experiment, the optical density of the overnight cultures was measured to
320 ensure that the MDCK cells were infected with a comparable multiplicity of infection (MOI)
321 across bacterial strains. For each strain, 1.2 mL was centrifuged at 2000 x g for 5 min, and washed
322 with 1 mL of DPBS. Bacterial pellets were resuspended in 16 mL of MEM. Host cells were
323 washed with MEM once, infected with 0.5 mL of bacterial mix per Transwell, and incubated at 37
324 °C for 10 min. The unused bacterial mix was serially diluted and plated onto BHI agar plates
325 containing 200 μg/mL streptomycin for bacterial enumeration. Transwells were washed three
326 times with MEM alone, then basal and apical media were both replaced with MEM + 10% FBS,
327 and plates were incubated at 37 °C for 1 h to allow bacterial invasion, followed by replacement
328 with MEM + 10% FBS + 50 μg/mL gentamicin to kill extracellular bacteria, and incubated at 37
329 °C for 15 min more. To assess subsequent transcytosis, Transwells were washed three times with
330 MEM + 10% FBS, and were then transferred to a new 12-well plate containing 1 mL of fresh
331 MEM + 10% FBS per well. This plate was incubated at 37 °C for 1 h, at which point basal media
332 was collected, vortex vigorously and 100 μL of each sample plated onto BHI agar plates
333 containing 200 μg/mL streptomycin. This step served as a negative control to exclude for
334 damaged monolayers. Meanwhile, the Transwells were transferred to another new 12-well plate
335 containing fresh MEM + 10% FBS per well. After an additional 3 h at 37 °C, basal media was
336 plated on BHI agar plates containing 200 μg/mL streptomycin as before, this time to assess true
337 transcytosis.

338 To quantify *L. monocytogenes* invasion, MDCK cells were seeded onto tissue culture-

339 treated 12-well plates at a density of $5x10^5$ cells per well three days prior to infection. MDCK cells

340 were then infected with an Δ*actA L. monocytogenes* strain expressing mTagRFP under the actA

341 promoter (37), which becomes transcriptionally active upon entry into the host cell cytoplasm.

342 Invasion was assayed with flow cytometry as previously described (38).

343 **RESULTS**

344 ***InlP binds afadin***

345 We attempted to find host binding partners for InlP in placental cells using a yeast two-
346 hybrid system to screen a human placenta library (39) (Supplementary Table 1). In parallel, we
347 used InlP fused to glutathione-S-transferase (InlP-GST) and a mass spectrometric approach to
348 pull-down and identify InlP binding partners in human placental tissue extracts (Supplementary
349 Fig. 1 and Supplementary Table 2). Both methods should in principle be able to detect both host
350 cell surface and cytoplasmic binding partners for InlP. While each of these approaches identified
351 multiple candidates, the protein afadin, encoded by the *MLLT4/AF-6* gene, was the only one
352 identified by both. Afadin is an F-actin-binding protein that also binds to the cytoplasmic domain
353 of the cell-cell adhesion molecule nectin, as well as to a wide variety of signaling proteins
354 including Src and multiple members of the Ras superfamily (40). Afadin has been shown to
355 contribute to the formation of cell-cell junctions during mouse embryonic development (41, 42)
356 and to apical constriction of adherens junctions during *Drosophila* morphogenesis (43). In
357 addition, afadin has been proposed to play multiple roles in cell polarization, migration,
358 differentiation, and oncogenesis (40).

359 We confirmed specific binding of InlP to afadin by pull-down experiments followed by
360 Western blot analyses (Fig. 1A and 1B). Elution fractions obtained after pull-down using an InlP-
361 GST fusion protein incubated with cell lysates from MDCK, MDCK *AF-6*$^{-/-}$ or human placental
362 villi were analyzed. Using anti-afadin antibodies, we detected afadin signal in the input fraction
363 and in the elution fractions after incubation of InlP-GST with protein extract from MDCK cell
364 lines (Fig. 1A) or from human placental villi (Fig. 1B). No afadin was detected in the elution
365 fractions when the GST control was used as bait (Fig. 1A and 1B). Confirming the specificity of

366 our antibodies, Western blot analysis on pull-down experiments performed using protein extract
367 from the afadin knock-out MDCK cell line did not show a detectable signal (Fig. 1A).
368 To determine the amount and spatial distribution of afadin present in human placental villi,
369 we performed immunofluorescence microscopy staining for afadin and observed that this protein
370 is very abundant in the placenta (Fig. 1C). Localization was primarily observed at the CTB layer
371 just beneath the syncytium, with small amounts in the stroma (see asterisk and arrow in Fig. 1C).
372 The high abundance of this potential InlP binding partner in the placenta, combined with our
373 previous report that InlP plays an important role in *L. monocytogenes* infection at the maternal-
374 fetal interface (1), are consistent with the hypothesis that InlP-afadin interactions are important for
375 the pathogenesis of placental infections.
376
377 ***Lmo2027 is a structural paralog of InlP that does not bind afadin***
378 The internalins that are predicted to be secreted by *L. monocytogenes* include InlC
379 (Lmo1786), InlP (Lmo2470), Lmo2027 and Lmo2445 (24). Of these, only InlC has been
380 extensively studied, but its primary sequence is not particularly similar to that of InlP (24%
381 sequence identity). The two other internalins predicted to be secreted, Lmo2027 and Lmo2445,
382 have not yet been characterized. Pairwise analyses of amino acid sequences indicated that InlP and
383 Lmo2445 are only 25% identical and 40% similar; however, InlP and Lmo2027 are much less
384 divergent, with 65% identity and 77% similarity (Fig 2A). Moreover, InlP and Lmo2027 share a
385 similar C-terminal domain that is not found in any of the other internalin family members (24).
386 Because of its high degree of sequence similarity to InlP, we decided to test whether Lmo2027
387 also binds afadin. As before, we performed pull-down assays with MDCK cell lysates, followed by
388 Western blots on elution fractions using Lmo2027-GST or InlP-GST fusion proteins as bait (Fig.

389 2B, C). Unlike InlP-GST, Lmo2027-GST did not enrich the afadin signal in the elution fractions
390 significantly more than the GST control. Even when diluted 10-fold, InlP-GST still pulled down
391 considerable afadin in comparison to the GST control and Lmo2027-GST. These results show that,
392 despite the relatively high sequence similarity of the two proteins, InlP, but not Lmo2027, binds
393 afadin.

394 To identify structural distinctions that might account for differences in afadin binding
395 affinity, we obtained 1.4 Å and 2.3 Å crystal structures of InlP and Lmo2027, respectively
396 (Supplementary Table 3). Analysis of the structures reveals that InlP and Lmo2027 generally
397 resemble previously characterized internalins (Fig 2D, E). Both proteins possess an N-terminal
398 domain that adopts the helical structure characteristic of internalins. This is followed by a concave
399 leucine rich-repeat (LRR) domain made up of 9 LRRs in InlP and 8 LRRs in Lmo2027 that can be
400 further subdivided into a "cryptic" portion consisting of 3 LRRs, which were not anticipated to
401 adopt an LRR-fold based upon bioinformatics analyses, and a "canonical" portion consisting of 6
402 LRRs in InlP and 5 LRRs in Lmo2027. Finally, the C-terminal domain in both proteins assumes
403 an immunoglobulin-like fold.

404 In particular, two features distinguish InlP and Lmo2027 from each other and from
405 previously characterized internalins. First, the additional LRR in InlP extends the LRR domain in
406 this protein as compared to Lmo2027 and increases the distance between the N-terminal and Ig-
407 like domains by ~4 Å. Such a fundamental distinction in the dimensions of the internalin could
408 affect whether a prospective binding partner could dock to and bind the LRR. Second, the concave
409 surface of previously crystallized internalin LRRs present an unbroken β-sheet (24), but in InlP
410 and Lmo2027 the third cryptic LRR (3rd LRR loop) protrudes, adopting a twisted conformation
411 that disrupts the continuity of this surface. Since this region in other LRR proteins is generally

412 involved in engaging the protein binding partner (22, 44), the distinct 3rd LRR loop seems well
413 situated to play a role in conferring binding specificity.
414 Unexpectedly, a calcium ion (from the crystallization solution) bound to the center of the
415 3rd LRR loop structure in InlP, but not Lmo2027 (Fig. 2D, E; Supplementary Fig. 2A), suggesting
416 that a calcium-stabilized loop conformation might be relevant for InlP protein-protein interactions.
417 Two of the residues specifically involved in coordination of the calcium ion in the InlP crystal
418 structure, D132 and G135, are not conserved in Lmo2027 (changed to T and E respectively). To
419 examine the interaction between InlP and calcium, we performed isothermal calorimetry
420 experiments, and found that calcium binds with a relatively low affinity of 35 μM (Supplementary
421 Fig. 2B).
422
423 ***InlPΔLRR5 has reduced afadin binding affinity***
424 Based on the alignment shown in Fig. 2A, it is evident that the main differences between
425 InlP and Lmo2027 are amino acid differences in that cluster to the C-terminal domain, as well as
426 the absence of 22 amino acid residues of Lmo2027 corresponding to one of the LRR motifs of
427 InlP. Given the high sequence similarity of the 6 "canonical" LRR motifs, it is difficult to
428 definitively identify which one is missing in Lmo2027, even if the pairwise alignment between
429 InlP and Lmo2027 suggests that the missing LRR motif might be LRR7. Therefore, we decided to
430 systematically delete individual LRR motifs in the InlP protein and test the effect of these
431 deletions on the protein's ability to bind afadin. We successfully generated three InlP deletion
432 mutants—InlPΔLRR5-GST, InlPΔLRR7-GST and InlPΔLRR8-GST—lacking the LRR5 (Δamino
433 acids 174-195), the LRR7 (Δamino acids 218-239) and the LRR8 (Δamino acids 240-261) motifs,

434 respectively. Each of these was then used as bait in pull-down experiments with MDCK cell
435 lysates, followed by Western blot analysis of the elution fractions to detect afadin.
436 Resins prepared using *E. coli* lysate expressing InlPΔLRR7-GST (Fig. 3A) pulled down
437 afadin from MDCK cell lysates with an efficiency roughly comparable to that observed for InlP-
438 GST (Fig. 3B). In contrast, we detected lower amounts of afadin in the pull-down fraction when
439 lysate from *E. coli* expressing the InlPΔLRR5-GST fusion protein was used to prepare the resin
440 (Fig. 3B). As the expression level of the InlPΔLRR5-GST fusion protein in *E. coli* appeared to be
441 somewhat lower than that of either InlP-GST or GST alone (Fig. 3A), we also performed a
442 Western blot comparing the elution fractions after five-fold dilution for both InlP-GST and GST
443 with no dilution for the InlPΔLRR5-GST elution fraction. Even compared to diluted InlP-GST,
444 substantially less afadin was detected in the sample for InlPΔLRR5-GST (Fig. 3C). This suggests
445 that deletion of the LRR5 motif decreases the affinity of afadin by at least ten-fold. The solubility
446 of the InlPΔLRR5-GST recombinant fusion protein was confirmed by dynamic light scattering
447 analysis (data not shown), consistent with the hypothesis that this reduction in apparent binding
448 affinity is due to specific structural alterations in the LRR domain. The InlPΔLRR8-GST was
449 expressed in *E. coli* lysates at ~30% of InlP-GST levels prepared under similar conditions
450 (Supplementary Fig. 3A). While we did observe reduced afadin binding by resins prepared using
451 *E. coli* lysates containing this fusion protein as compared to native InlP-GST (Supplementary Fig.
452 3B), this decrease was approximately proportional to the reduction in expression level. Overall
453 this analysis suggested that InlPΔLRR5 represents a useful mutant for interrogating the InlP-
454 Afadin interaction.
455 To examine the effects of the InlPΔLRR5 mutation on binding to host proteins, we used a
456 GST control, InlP fused to GST (InlP-GST) or InlPΔLRR5 fused to GST (InlPΔLRR5-GST) as

457 baits and identified proteins pulled down from MDCK epithelial cell lysates by mass spectrometry
458 (Fig. 3D and Supplementary Table 2). Of the MDCK cell proteins found specifically to bind InlP-
459 GST, only afadin (*MLLT4/AF-6*) had also been identified in the screens described above using
460 yeast two-hybrid screening on a human placental library (Supplementary Table 1) and mass
461 spectrometry of proteins pulled down from human placental tissue extracts (Supplementary Table
462 2). Consistent with the Western blot analysis, mass spectrometry analysis confirmed that afadin
463 associated much less strongly with InlPΔLRR5-GST than with InlP-GST (Fig. 3D and
464 Supplementary Fig. 4). These findings are consistent with the hypothesis that the InlPΔLRR5
465 mutant is specifically deficient in interacting with afadin in MDCK cells, while otherwise
466 retaining much of its normal structure and protein-protein interaction potential.
467
468 ***Afadin-InlP interactions decrease the attachment of epithelial cells to the extracellular***
469 ***matrix, but not adhesion between adjacent epithelial cells***
470 We sought to investigate whether the interaction between InlP and afadin could alter the
471 structural integrity of epithelial cell monolayers in ways that might facilitate *L. monocytogenes*
472 invasion or cell-to-cell spread. To test whether InlP affects the integrity of cell-cell junctions in a
473 monolayer, we constructed a line of MDCK cells that could express a humanized version of InlP
474 after induction by doxycycline (MDCK-InlP^{+}). We cultured wild-type MDCK, MDCK *AF-6*$^{-/-}$, and
475 MDCK-InlP cells on Transwell filters for three days and measured the permeability of the cell
476 monolayers using inulin-FITC. As expected after deletion of a protein necessary for proper
477 formation of adherens junctions and tight junctions (41), MDCK *AF-6*$^{-/-}$ monolayers showed a
478 substantial increase in permeability to inulin relative to wild-type MDCK monolayers. However,
479 MDCK-InlP monolayers showed low permeability, comparable to the baseline level for wild-type

480 MDCK monolayers, both with and without induction of the InlP transgene using doxycycline
481 (Fig. 4A). This result suggests that the interaction between InlP and afadin does not inhibit the
482 ability of afadin to perform its normal function in establishment and maintenance of impermeable
483 cell-cell junctions.

484 Next, we used these cell lines to examine the modulation of cell-substrate interactions by
485 InlP binding to afadin. To this end, we also generated a line of MDCK *AF-6*$^{-/-}$ cells with the
486 doxycycline-inducible InlP transgene. We used traction force microscopy (TFM) to measure the
487 ability of MDCK cells to generate traction forces on their substrates with and without expression
488 of Afadin and/or InlP. Uninduced MDCK-InlP cell monolayers without doxycycline (the positive
489 control) grown on deformable substrates as confluent, polarized monolayers were able to generate
490 significant strain energy on the order of 100-200 nN·μm (Fig. 4B, C) and to exert traction stresses
491 with peak values around 100 Pa, comparable to previous reports (45, 46). Both the induction of
492 the InlP transgene and the deletion of afadin caused a substantial reduction in strain energy.
493 Induction of InlP expression in the background of the MDCK *AF-6*$^{-/-}$ cell line did not lead to any
494 further reduction, consistent with the hypothesis that the primary effect of InlP expression on
495 abrogation of traction force generation in MDCK cells is due to its interaction with afadin.

496 We have previously demonstrated that a decrease in monolayer traction force can be
497 caused either by a direct inhibition of cell-substrate interactions or by an indirect inhibition of
498 lateral tension at cell-cell junctions in the monolayer (33). To distinguish between these two
499 possibilities, we also performed TFM for isolated cells under the same four conditions. Just as for
500 the monolayers, either the expression of InlP or the deletion of *AF-6* caused a significant decrease
501 in the ability of isolated individual cells to generate traction force (Fig. 4D, E). Taken together,
502 these results suggest that the InlP-afadin binding interaction specifically disrupts afadin's normal

503 activity in enhancing traction force generation at the cell-substrate interface but has no effect on
504 afadin's normal function at cell-cell junctions in the monolayer.
505
506 ***InlP enhances L. monocytogenes transcytosis through MDCK polarized monolayers***
507 Finally, we examined the influence of the InlP-afadin interaction on infection and spread
508 of *L. monocytogenes* in MDCK monolayers. We infected wild-type and MDCK *AF-6*$^{-/-}$ cells with
509 wild type or *ΔinlP L. monocytogenes*. Gentamicin was added at 30 min to kill extracellular
510 bacteria, and remaining intracellular bacteria were enumerated at 2, 5, 8 and 24 h post-infection.
511 At 2 h, the MDCK *AF-6*$^{-/-}$ cells harbored ~10 times the number of bacteria as compared to wild-
512 type MDCK cells, although the rate of intracellular growth of the bacteria was unchanged.
513 Deletion of *inlP* had no significant effect on invasion or intracellular replication of *L.*
514 *monocytogenes* in either host cell background (Fig. 5A).
515 The observation that MDCK *AF-6*$^{-/-}$ monolayers had substantially more intracellular
516 bacteria at early time points in the course of infection as compared to wild-type MDCK cells
517 raised the possibility that the deletion of *AF-6* caused an increase in the efficiency of *L.*
518 *monocytogenes* invasion. Because the cell receptor for *L. monocytogenes* invasion into epithelial
519 cells, E-cadherin, is normally sequestered from the apical surface of cells in well-polarized,
520 confluent monolayers, invasion under such circumstances is rare and typically takes place at sites
521 of local, transient disruption of the epithelial cell-cell junctions, for example at sites of extrusion
522 of apoptotic cells (8). Consequently, any disruption of normal cell-cell junctions in epithelial
523 monolayers typically increases the efficiency of *L. monocytogenes* invasion (38). To determine if
524 this was the reason for the increased bacterial load in MDCK *AF-6*$^{-/-}$ monolayers at early time
525 points, we infected both wild-type and *AF-6*-knockout MDCK cells with *ΔactA L. monocytogenes*

526 expressing mTagRFP under the *actA* promoter and counted the number of RFP-positive host cells
527 by flow cytometry 5 h post-inoculation, which represents the number of bacteria-containing cells.
528 Because these bacteria are not capable of actin-based cell-to-cell spread, this assay allows
529 determination of the number of directly invaded host cells, independent of any later variations in
530 bacterial spread (47). Indeed, we found approximately 6-fold more invasion of MDCK *AF-6*$^{-/-}$ cells
531 with *L. monocytogenes* as compared to wild-type MDCKs (Fig. 5B).

532 Our previous work demonstrated that wild-type and *ΔinlP L. monocytogenes* form foci of
533 similar size in MDCK monolayers (1), suggesting that horizontal cell-to-cell spread in a polarized
534 epithelium is not affected by InlP. This is corroborated by our findings here that the InlP-afadin
535 interaction does not disrupt the function of afadin at cell-cell junctions. However, we also showed
536 that *ΔinlP* strains are impaired in spreading from the CTB epithelial layer into the placental
537 stroma (1), and here we have found that the InlP-afadin interaction specifically disrupts the
538 mechanics of MDCK cell traction force generation at the cell-substrate interface (Fig. 4). We
539 therefore wondered whether this protein-protein interaction might specifically affect the ability of
540 intracellular *L. monocytogenes* to use actin-based motility to spread through the basal face of the
541 CTB epithelial monolayer underlying the placental STB, rather than horizontally through the
542 lateral faces of neighboring CTB epithelial cells. We designed an assay to mimic this particular
543 type of spread by growing MDCK cells on Transwell filters with large (3 μm) pores through
544 which bacterial protrusions could extend into the lower well. Under these culture conditions,
545 MDCK cells form well-polarized monolayers and secrete a thick and well-organized basement
546 membrane (basal lamina) (48), so bacterial protrusions reaching the lower well must have been
547 able to form at the basal side of the cell and push through the basement membrane. Approximately
548 5 hours after inoculation from the apical side, bacteria that had successfully performed

549 transcytosis through the monolayer were collected from the lower well. In this assay, *ΔactA*
550 bacteria exhibited a substantial (>10-fold) reduction in transcytosis, demonstrating that this
551 process is dependent on bacterial actin-based motility (Fig. 5C). The *ΔinlP* strain also showed a
552 statistically significant reduction in transcytosis (~4-fold), consistent with the hypothesis that the
553 InlP-afadin interaction specifically alters cell mechanics at the basal cell-substrate interface and
554 thereby facilitates *L. monocytogenes* spread in a direction perpendicular to the monolayer.
555 If the nature of the InlP-afadin interaction were simply to sequester or inhibit afadin's
556 normal activity at the basal surface, we would expect that deletion of *AF-6* in the host cells should
557 be able to rescue the transcytosis defect of *ΔinlP L. monocytogenes*. Interestingly, however, this
558 was not the case. MDCK *AF-6*$^{-/-}$ monolayers infected with wild-type bacteria exhibited an
559 unexpected decrease in transcytosis efficiency, resulting in about two-fold fewer bacteria reaching
560 the lower well as compared to parallel infections in wild-type MDCK cells, despite the much
561 higher efficiency of initial invasion (Fig. 5C). In this host cell background, transcytosis of *ΔinlP*
562 bacteria was slightly less efficient than that of wild-type bacteria, in contrast to the expected
563 phenotypic rescue.
564 We wished to confirm that this unexpected observation could be attributed specifically to
565 the InlP-afadin interaction, rather than to some pleiotropic effect of *AF-6* deletion in the MDCK
566 cells, and so took advantage of our earlier determination that the InlPΔLRR5 mutation specifically
567 disrupts afadin binding (Fig. 3 and Supplementary Table 2). Infection of wild-type MDCK cells
568 with *L. monocytogenes* expressing the mutant InlPΔLRR5 resulted in a transcytosis defect
569 comparable to the defect of the complete *ΔinlP* deletion in parallel experiments (Fig. 5D). We
570 conclude that the InlP-afadin protein-protein interaction exerts a specific effect to enhance

571 transcytosis of *L. monocytogenes* through the basal face of polarized epithelial cells that is not

572 equivalent to the simple removal or sequestration of afadin from this site.

573 **DISCUSSION**

574 En route to infection of the fetus, *L. monocytogenes* experiences multiple bottlenecks,
575 from trafficking to the placenta (3) to surviving the placental innate immune defenses (49) to
576 crossing the trophoblast monolayer and its associated basement membrane into the fetal stroma
577 and fetal circulation (20). InlP initially attracted our interest due to its identification in a screen for
578 *L. monocytogenes* mutants that were defective in their ability to infect the placenta (1). Two
579 unbiased screening methods to identify potential placental binding partners, a yeast two-hybrid
580 screen using a placental cDNA library and mass spectrometric identification of human proteins
581 pulled down by InlP from placental extracts, converged on afadin as a significant candidate
582 binding partner. Afadin is not found on the cell surface, but instead is primarily associated with
583 the cytoplasmic face of cell-cell junctions containing nectin (41, 53). Therefore, it seems likely
584 that InlP is most helpful in breaching that third barrier and accessing the fetal stroma.

585 Of the 25 known members of the *L. monocytogenes* internalin family, the only other one
586 known to have host cell cytoplasmic binding partners involved in its virulence functions is InlC.
587 InlC binds to one of the subunits of the IκB complex thereby modulating the host cell innate
588 immune response (54). In addition, InlC also binds the adapter protein Tuba, which cooperates
589 with the actin polymerization regulator N-WASP to modulate tension at cell-cell junctions and
590 thereby promote *L. monocytogenes* cell-to-cell spread in epithelial monolayers (55). Intriguingly,
591 InlC and InlP are two of only four internalin family members that are thought to be secreted in a
592 soluble form rather than anchored to the bacteria cell surface (24). As more internalin family
593 members are characterized, it will be interesting to see whether the trend persists of surface-
594 anchored internalins binding to host cell surface proteins and secreted internalins binding to host
595 cell cytoplasmic proteins.

596 While we have not determined the structure of the InlP-afadin complex, our work does
597 give some clues into the likely nature of this interaction. The internal in-frame deletion mutant
598 InlP-ΔLRR5, which lacks one of the leucine-rich repeats, binds afadin less well than full length
599 InlP, but this is probably not simply due to the shorter overall size of the concave face of the LRR
600 domain because InlP-ΔLRR7 and InlP-ΔLRR8, which should have a similar overall length of the
601 LRR domain concave face, seem to have little or no deficiency in afadin binding. It is thus likely
602 that there are specific residues in LRR5 that stabilize the interaction. An interesting unanswered
603 question concerns the role of the unusual protruding loop from LRR3 in determining binding
604 partner specificity. Although we found that this loop between amino acids 132-136 in the InlP
605 structure bound Ca^{2+} with an affinity of 35 μM, this binding affinity is probably too weak to be
606 relevant in the host cell cytoplasm where the Ca^{2+} concentration rarely rises above ~2 μM (56).
607 This is not the case for other subcellular compartments like the acidifying phagosomes, where the
608 Ca^{2+} concentration has been shown to be >70 μM (56). Thus, it is possible that calcium binding by
609 InlP plays a role during *L. monocytogenes* escape from the primary (single-membrane) or
610 secondary (double-membrane) vacuole. It should be noted that Shaughnessy et al. (57) observed
611 that listeriolysin O pores generated by the bacterium in the process of primary vacuolar escape
612 allow Ca^{2+} in the vacuole to leak into the cytoplasm, albeit slowly. It is possible that calcium
613 binding promotes changes in InlP behavior that are specific to different calcium microdomains in
614 the polarized epithelium (58, 59), including microdomains potentially specific to basal protrusions
615 and/or placental trophoblasts (60).
616 Other bacterial pathogens are also known to secrete virulence factors into the host cell
617 cytoplasm that modulate host cell biology in ways that benefit bacterial survival or spread (33, 61-
618 64). One particularly relevant example is the virulence factor Sca4, secreted by *Rickettsia parkeri*.

619 Analogous to InlC, Sca4 binds the host protein vinculin at cell-cell junctions and alters cortical
620 tension, promoting actin-based cell-to-cell spread of the bacterium horizontally through host cell
621 monolayers (33). Given the precedent that both InlC and Sca4 bind to proteins that perform
622 scaffolding functions at cell-cell junctions in polarized epithelia (Tuba and vinculin respectively)
623 and modulate cortical tension to promote bacterial spread, our initial expectation on discovering
624 that InlP binds the cell-cell junction-associated protein afadin was that its mechanism of action
625 would be similar. However, we have found no evidence that InlP has any effect on cell-cell
626 junctions in the host monolayer, or indeed that it makes any significant contribution to lateral
627 actin-based spread of *L. monocytogenes* within the horizontal plane of the monolayer.
628 Instead, our results indicate that the relevant site of action of InlP in the host cell is the
629 basal face, not the lateral face, and that the InlP-afadin interaction specifically modulates the
630 nature of the host cell organization at the basal face or interaction with the underlying basement
631 membrane in a way that promotes *L. monocytogenes* spread that is perpendicular, rather than
632 parallel to the monolayer. Afadin has not been described as being localized to the basal face of
633 polarized epithelial cells, or to cell-ECM junctions; instead its functional characterization has
634 focused primarily on nectin binding at cell-cell junctions (40, 41). Conditional knockouts in the
635 mouse intestine lead to increases in intestinal permeability (65), consistent with the phenotype we
636 have described here of afadin loss causing permeabilization of cell-cell junctions in MDCK cells.
637 Whether afadin also plays a role in cell-ECM connections is unclear, but in certain cell types,
638 removal of afadin can enhance cell migration (66) and invasive capacity (67), or suppress
639 neuronal axon branching (68). While these cellular behaviors might involve specific changes in
640 cell-ECM interactions, it is also likely in these cases that the effects of afadin disruption are

641 mediated indirectly through its interactions with critical signaling molecules, Rap1, Src and R-Ras
642 respectively (66-68).
643 How does InlP binding modulate afadin activity at the basal face of epithelial cells? For
644 both InlC and Sca4, deletion of the host cell binding partner is sufficient to (partially) rescue the
645 bacterial deletion phenotype, consistent with the simple idea that binding of the bacterial virulence
646 factors to their host cell partners effectively inhibits or sequesters those host cell partners (33, 55).
647 In contrast, our results indicate that the consequences of the interaction between InlP and afadin
648 are more complex than simple sequestration. InlP expression in uninfected MDCK cell
649 monolayers has no effect on integrity of cell-cell junctions, while deletion of afadin results in a
650 significant increase in monolayer permeability, so the presence of InlP does not appear to disrupt
651 afadin's normal activities at the cell-cell junctions. In contrast, expression of InlP phenocopies
652 afadin deletion with respect to the ability of epithelial cells to generate traction forces on their
653 substrates. And most intriguingly we have found that *AF-6* knockout MDCK cells are less able to
654 support transcytosis of both wild-type and *ΔinlP L. monocytogenes* across the basement
655 membrane than are wild-type host cells; if afadin normally simply strengthens the cell-substrate
656 interface then the *AF-6* knockout host cells should be more permissive for bacterial transcytosis,
657 rather than less. This raises the interesting possibility that the InlP-afadin binding interaction
658 results in a novel activity that specifically promotes bacterial formation of actin-based protrusions
659 at the cell basal face.
660 In the context of placental infection, the spatial specificity for the activity of the InlP-
661 afadin interaction at the basal face of polarized epithelial cells is relevant, as our previous work
662 has suggested that vertical spread from the CTB monolayer into the underlying fetal stroma is a
663 major barrier for infection of the fetus (1, 20, 69). However, we previously showed that the Δ*inlP*

664 mutant is not impaired in reaching the liver or spleen in orally-infected guinea pigs (1), raising the
665 question of why the phenotype is apparently specific for placental infection when enhanced
666 transcytosis through the basement membrane should also be relevant for *L. monocytogenes*
667 crossing the intestinal epithelium or crossing the endothelial cells in blood vessels to invade the
668 liver. In this context, we note that the intestinal barrier is organized differently from that of the
669 placenta. The intestinal epithelium is rich in intercellular junctions that link neighboring cells
670 together, while the placental syncytiotrophoblast that contacts maternal blood is a single,
671 continuous plasma membrane extending over tens of thousands of square millimeters in later
672 stages of human gestation. The invasive cytotrophoblasts in the uterine decidua do have exposed
673 lateral surfaces and cell-cell junctions, but they lack the lymphatic and immune components of the
674 intestine in that there are no Peyer's Patches and M cells with phagocytic and migratory
675 capabilities. While some white blood cells do traffic across this barrier in both directions (70),
676 traffic is likely more limited than in the mucosal-associated lymphoid tissues of the gut. The lack
677 of a role for InlP in crossing the intestinal barrier is therefore consistent with earlier work showing
678 that *L. monocytogenes* traffics from the gut to the bloodstream by being carried by immune cells
679 (71). In this context, the limited immune cell traffic observed across the placental barrier might
680 explain how *ΔinlP L. monocytogenes* are impaired in crossing the subsyncytial CTB monolayer—
681 undergirded by a basement membrane—into the fetal stroma (1). Alternatively, it is possible that
682 the basement membrane underlying the CTB layer simply presents a more formidable physical
683 barrier than that found underneath the intestinal epithelium. An interesting issue, to be addressed
684 in future work, is whether there is impairment in the invasion of *ΔinlP L. monocytogenes* across
685 the blood-brain endothelial barrier.

686 For decades, *L. monocytogenes* has been a useful tool for the study of mammalian cells,
687 barriers, and immune functions. Increasingly, its capacity to reveal basic knowledge about higher
688 levels of biological organization—mammalian tissues and organs—is becoming evident. Through
689 investigations of how bacteria cross barriers and of the interactions between bacterial factors and
690 host pathways, we learn not only more about what regulates pathogenesis, but about the structures
691 of these tissues themselves, in how they are generated, their composition, and how they can be
692 disrupted.

693 **AUTHOR CONTRIBUTIONS:**

694 C.F. and A.I.B. conceived the project and initiated collaborations with the other authors.
695 C.F. generated all bacterial mutant strains and mammalian cell lines. C.F., E.E.B., F.E.O., S.H.L.,
696 G.R., and S.N. performed experiments and/or analyzed data. W.F.A., J.A.T. and A.I.B. provided
697 resources and supervision. C.F., E.E.B., J.R.R., A.I.B. and J.A.T. wrote the paper.

698

699 **ACKNOWLEDGEMENTS:**

700 Our thanks to Henriette Macmillan, Cedric Brimacombe, George Minasov, Olga
701 Kiryukhina and Albin Cardona-Correa for discussions and experimental support, as well as tissue
702 donors who provided informed consent. This work was supported by NIH R01AI084928 (A.I.B),
703 Burroughs Wellcome Fund (A.I.B), NIH R01AI036929 (J.A.T), HHMI (J.A.T), the HHMI
704 Gilliam Fellowship for Advanced Study (F.E.O.), the Stanford Graduate Fellowship (F.E.O.), the
705 American Heart Association (E.E.B.), NIH F32AI108195 (G.R.), Society for Pediatric Pathology
706 Young Investigator Research grant (G.R.), and the University of California Partnerships for
707 Faculty Diversity President's Postdoctoral Fellowship (G.R.). Flow cytometry was performed at
708 the Stanford Shared FACS Facility. The Center for Structural Genomics of Infectious Diseases
709 has been funded with federal funds from the National Institute of Allergy and Infectious Diseases,
710 National Institutes of Health (NIH), Department of Health and Human Services, under Contract
711 Nos. HHSN272200700058C and HHSN272201200026C (to W.F.A). This research used resources
712 of the Advanced Photon Source, a U.S. Department of Energy (DOE) Office of Science User
713 Facility operated for the DOE Office of Science by Argonne National Laboratory under Contract
714 No. DE-AC02-06CH11357. Use of the LS-CAT Sector 21 was supported by the Michigan

Economic Development Corporation and the Michigan Technology Tri-Corridor (Grant 085P1000817).

718 **FIGURE LEGENDS**

719 **Figure 1. Bacterial effector InlP binds host adaptor protein afadin.** (A-B) InlP-GST fusion
720 protein (InlP) or GST protein alone (-) bound to glutathione-Sepharose resin were incubated
721 overnight with protein extracts from (A) MDCK or MDCK *AF-6*$^{-/-}$ cells or (B) human placenta.
722 Input (IN) and elution fractions (EF) were analyzed by Western blot with anti-afadin antibodies.
723 Actin: loading control. (C) Immunofluorescence of human placental villi stained for afadin (red)
724 and DAPI (blue), white bar =10 μm (right). Asterisk labels a portion of the stroma, and the arrow
725 points to some of the CTBs.

726

727 **Figure 2. Distinct features of InlP as compared to Lmo2027.** (A) Pairwise sequence alignment
728 of InlP and Lmo2027 with conserved amino acids highlighted in red. The LRRs and calcium
729 binding site on InlP are noted. Arrows signify ß-sheets and coils correspond to α-helices. (B)
730 Loading control of pull down experiments on Lmo2027 by Coomassie blue staining. GST protein
731 alone (-), Lmo2027-GST fusion protein (2027) or InlP-GST fusion protein (InlP) bound to
732 glutathione-Sepharose resin used as bait for pull-down experiments with protein extracts from
733 MDCK cells. The elution fraction from pull-down samples using InlP-GST (InlP) as bait were
734 sequentially diluted 5-fold before SDS analysis; undiluted elution fractions were analyzed from
735 pull-down samples using GST (-) or Lmo2027 (2027). Data shown are Coomassie staining and the
736 most abundant band in each lane represents the bait. (C) GST fusion proteins or GST protein
737 alone (-) bound to glutathione-Sepharose resin were incubated overnight with protein extracts
738 from MDCK cells, and elution fractions were analyzed by Western blot with anti-afadin
739 antibodies. The following GST fusion proteins were used: GST-Lmo2027 (Lmo2027) and GST-
740 InlP (InlP). Undiluted elution fractions were analyzed with the exception of the elution fractions

741 marked by black triangles: elution fractions from the experiments using GST-InlP as bait were
742 sequentially diluted by 5-fold before western blot analysis. Actin: loading control. (D) Crystal
743 structure of InlP with schematic depiction of domain layout below. (E) Crystal structure of
744 Lmo2027 with color-coded domains, like in (D).
745
746 **Figure 3. LRR5 stabilized afadin- InlP interaction.** (A) Loading control of InlP-afadin
747 binding pull-down experiments with LRR mutants by Coomassie blue staining. GST protein alone
748 (-), InlPΔLRR5-GST fusion protein (ΔLRR5), InlPΔLRR7-GST fusion protein (ΔLRR7), or InlP-
749 GST (InlP) bound to glutathione-Sepharose resin were used as bait for pull-down experiments
750 with protein extracts from MDCK cell line. Data shown are Coomassie staining, and the most
751 abundant band in each lane represents the bait. (B-C) GST fusion proteins or GST protein alone (-
752) bound to glutathione-sepharose resin were incubated overnight with protein extracts from
753 MDCK cells, and elution fractions (EF) were analyzed by Western blot with anti-afadin
754 antibodies. The following GST fusion proteins were used: GST-InlP (InlP) and GST-InlP with
755 deletions in LRR5 (ΔLRR5) or LRR7 (ΔLRR7). Actin: loading control. Undiluted elution
756 fractions were analyzed with the exception of the elution fractions marked in panel C that were
757 diluted 5-fold. Actin: loading control. (D) Scatter plot of the logarithm of the ratio of intensity of
758 InlP-GST bound proteins to the intensity of ΔLRR5-GST bound proteins versus total intensity of
759 InlP-GST bound proteins. The intensities (A.U.) of the proteins were identified through mass
760 spectrometry using InlP-GST or InlPΔLRR5-GST as baits to identify host binding partners in the
761 MDCK cell culture extracts. Blue diamonds show all the proteins apart from afadin, which is
762 indicated as orange square. Using this metric, afadin is 2.7 standard deviations away from the
763 mean for this group.

764

765 **Figure 4. Cell-ECM traction stresses decrease in magnitude when afadin is not expressed or**
766 **when InlP is present.** (A) MDCK, MDCK *AF-6*$^{-/-}$, and MDCK cell lines stably transfected with
767 *inlP* under a doxycycline (DOX) inducible promoter were grown on Transwell filters for three
768 days until formation of polarized epithelia. Inulin-FITC was added to the upper compartment of
769 the Transwell insert. The cell permeability was analyzed at different time points by measuring the
770 fluorescence intensity in the lower compartment. MDCK InlP^{-} and MDCK InlP^{+}: stably
771 transfected cells without or with InlP expression secondary to doxycycline exposure for 24 h prior
772 to the addition of Inulin-FITC. (B) Representative phase images (first row) and maps showing the
773 magnitude of traction stresses of confluent MDCK monolayers adherent to hydrogels coated with
774 collagen I (color indicates stress magnitude in Pa). Columns refer to: MDCK InlP^{-}, MDCK InlP^{+},
775 MDCK *AF-6*$^{-/-}$ InlP^{-} and MDCK *AF-6*$^{-/-}$ InlP^{+}. Scale bar corresponds to 20 μm. (C) Time-
776 averaged strain energy (nN•μm) calculated for multiple regions within confluent MDCK
777 monolayers. Boxplots refer to N=11 MDCK InlP^{-}, N=11 MDCK InlP^{+}, N=12 MDCK *AF-6*$^{-/-}$ InlP^{-}
778 , N= 12 MDCK *AF-6*$^{-/-}$ InlP^{+} monolayer regions. (D-E) TFM results for single cells adherent to
779 polyacrylamide hydrogels coated with collagen I. (D) Instantaneous maps showing the magnitude
780 of traction stresses (color indicates stress values in Pa). Columns refer to: MDCK InlP^{-}, MDCK
781 InlP^{+}, MDCK *AF-6*$^{-/-}$ InlP^{-} and MDCK *AF-6*$^{-/-}$ InlP^{+}. Cell outlines are in white. Scale bar
782 corresponds to 20 μm. (E) Time-averaged strain energy (nNμm) from individual cells. Boxplots
783 refer to N=15 MDCK InlP^{-}, N=17 MDCK InlP^{+}, N= 15 MDCK *AF-6*$^{-/-}$ InlP^{-}, and N=18 MDCK
784 *AF-6*$^{-/-}$ InlP^{+}. For boxplots in (C), (E) circles represent outliers, and the boxplots' notched sections
785 show the 95% confidence interval around the median (Wilcoxon–Mann–Whitney test). One or

786 two asterisks denote statistically significant differences between the medians of two distributions
787 (<0.05 or <0.01, respectively; Wilcoxon rank sum test).
788
789 **Figure 5. InlP enhances transcytosis through MDCK polarized monolayers**. (A) Intracellular
790 growth curves of wild type 10403S *L. monocytogenes* in MDCK (black solid line) or MDCK *AF-*
791 *6*$^{-/-}$ (black dashed line) cells and of Δ*inlP L. monocytogenes* in MDCK (gray solid line) or MDCK
792 *AF-6*$^{-/-}$ (gray dashed line) cells. Unpolarized monolayers of MDCK cell lines were infected with
793 10403S at MOI of 150:1. Gentamicin was added at 50 μg/ml to kill extracellular bacteria and
794 maintained in media thereafter. Each growth curve represents the means and standard deviations
795 of colony forming units (CFU) over time from three separate experiments performed in
796 triplicates. (B) Afadin limits initial *L. monocytogenes* invasion. Flow cytometry quantifying the
797 number of *L. monocytogenes*-containing MDCK and MDCK *AF-6*$^{-/-}$ cells 5 hours post infection.
798 Data were normalized to 1 for wild-type MDCK cells infected with Δ*actA L. monocytogenes* for
799 each experiment, and pooled from two independent experiments (each experiment is depicted by
800 different symbols). (C) Amount of transcytosis by wild-type (blue), Δ*inlP* (red), and Δ*actA*
801 (green) *L. monocytogenes* through MDCK and MDCK *AF-6*$^{-/-}$ monolayers. Data were normalized
802 to 1 for MDCK cells infected with wild-type *L. monocytogenes* for each experiment, and pooled
803 from four independent experiments (MDCK cells) or three independent experiments (MDCK
804 *AF-6*$^{-/-}$ cells). Each experiment is depicted by different symbols. (D) Amount of transcytosis by
805 wild-type, Δ*inlP*, and ΔLRR5 *L. monocytogenes* through MDCK monolayers. Data were
806 normalized to 1 for MDCK cells infected with wild-type *L. monocytogenes* for each experiment,
807 and pooled from three independent experiments. Each experiment is depicted by different
808 symbols.

809

810 **SUPPORTING INFORMATION CAPTIONS**

811 **Figure S1. Coomassie and silver stains showing fractions for mass spectrometry analysis.**
812 GST protein alone and InlP -GST fusion protein bound to glutathione-Sepharose resin were used
813 as bait for pull-down experiments with (+) or without (-) protein extracts from human placenta.
814 Shown on the left is Coomassie blue staining of each fraction, with the most abundant band in
815 each lane representing the bait protein. Shown on the right is silver staining of each fraction, with
816 the most abundant band in each lane representing the bait protein. The red boxes labeled A and B
817 show the two fractions extracted from gel and analyzed by mass spectrometry (see Sheet 1 and 2
818 in Supplementary Table 2).

819

820 **Figure S2. Structural and biochemical details on InlP Ca^{2+} interaction.** (A) Schematic view of
821 the interaction between the Ca^{2+} with the 3rd LRR loop of InlP. The amino acids D132 and E182,
822 which are involved in the interaction, are shown as sticks, water molecules as red spheres, and
823 hydrogen bonds as dashed lines. (B) Isothermal titration calorimetry results show Ca^{2+} binding to
824 InlP. The isotherm was fit by a one site binding model (N = 1.8 ± 0.1 site, K = 2.6E4 ± 6.5E3 M^{-1},
825 ΔH = -1176 ± 90.2 cal/mol, ΔS = 16.3 cal/mol/deg).

826

827 **Figure S3. Loading control by Coomassie staining and western blot analysis of pull down**
828 **experiments on InlPΔLRR8 mutant.** InlP-afadin binding pull-down experiments with ΔLRR8
829 mutant. GST protein alone (-), InlPΔLRR8-GST fusion protein (ΔLRR8), or InlP-GST (InlP)
830 bound to glutathione-sepharose resin were used as bait for pull-down experiments with protein
831 extracts from MDCK cell line. (A) Coomassie blue staining of each fraction, with the most

832 abundant band in each lane representing the bait protein. (B) Data shown are a western blot
833 analysis using anti-afadin antibodies. Actin was used as loading control.

834 **Figure S4. LRR5 stabilized afadin- InlP interaction.** Scatter plot of intensities of InlP-GST
835 versus ΔLRR5-GST binding proteins coming from MDCK cell cultures extracts. Plot shows the
836 sum of intensities (A.U.) of the proteins identified through mass spectrometry using InlP-GST or
837 InlPΔLRR5-GST as baits to identify host binding partners in the MDCK extracts. Blue diamonds
838 show all the proteins apart from afadin, which is indicated as orange square. Black line shows
839 X=Y. Filters applied to the data are discussed in the Methods section.

840

841 **SUPPLEMENTARY TABLES**

842 **Supplementary Table 1. Yeast two-hybrid screening of human placenta library.**

843 **Supplementary Table 2. Mass spectrometry data from pull-down of InlP-GST interacting**
844 **with binding partners from human placental tissue and from extracts from MDCK cell**
845 **cultures.**

846 **Supplementary Table 3. Crystallographic Table.**

847

848

849 **REFERENCES**

850 1. Faralla C, Rizzuto GA, Lowe DE, Kim B, Cooke C, Shiow LR, et al. InlP, a New
851 Virulence Factor with Strong Placental Tropism. Infect Immun. 2016;84(12):3584-96.
852 2. Janakiraman V. Listeriosis in Pregnancy: Diagnosis, Treatment, and Prevention. Reviews
853 in Obstetrics and Gynecology. 2008;1(4):179-85.
854 3. Robbins JR, Bakardjiev AI. Pathogens and the placental fortress. Curr Opin Microbiol.
855 2012;15(1):36-43.
856 4. Vázquez-Boland JA, Krypotou E, Scortti M. Listeria Placental Infection. mBio.
857 2017;8(3):e00949-17.
858 5. Vazquez-Boland JA, Kuhn M, Berche P, Chakraborty T, Dominguez-Bernal G, Goebel W,
859 et al. Listeria pathogenesis and molecular virulence determinants. Clin Microbiol Rev.
860 2001;14(3):584-640.
861 6. Mengaud J, Ohayon H, Gounon P, Mege RM, Cossart P. E-cadherin is the receptor for
862 internalin, a surface protein required for entry of L. monocytogenes into epithelial cells. Cell.
863 1996;84(6):923-32.
864 7. Lecuit M, Dramsi S, Gottardi C, Fedor-Chaiken M, Gumbiner B, Cossart P. A single
865 amino acid in E-cadherin responsible for host specificity towards the human pathogen Listeria
866 monocytogenes. Embo j. 1999;18(14):3956-63.
867 8. Pentecost M, Otto G, Theriot JA, Amieva MR. Listeria monocytogenes Invades the
868 Epithelial Junctions at Sites of Cell Extrusion. PLOS Pathogens. 2006;2(1):e3.
869 9. Tilney LG, Portnoy DA. Actin filaments and the growth, movement, and spread of the
870 intracellular bacterial parasite, Listeria monocytogenes. The Journal of Cell Biology.
871 1989;109(4):1597-608.
872 10. Robbins JR, Barth AI, Marquis H, de Hostos EL, Nelson WJ, Theriot JA. Listeria
873 monocytogenes exploits normal host cell processes to spread from cell to cell. J Cell Biol.
874 1999;146(6):1333-50.
875 11. Drevets DA, Jelinek TA, Freitag NE. Listeria monocytogenes-infected phagocytes can
876 initiate central nervous system infection in mice. Infect Immun. 2001;69(3):1344-50.
877 12. Bakardjiev AI, Theriot JA, Portnoy DA. Listeria monocytogenes traffics from maternal
878 organs to the placenta and back. PLoS Pathog. 2006;2(6):e66.
879 13. Portnoy DA, Auerbuch V, Glomski IJ. The cell biology of Listeria monocytogenes
880 infection: the intersection of bacterial pathogenesis and cell-mediated immunity. The Journal of
881 Cell Biology. 2002;158(3):409-14.
882 14. Le Monnier A, Autret N, Join-Lambert OF, Jaubert F, Charbit A, Berche P, et al. ActA is
883 required for crossing of the fetoplacental barrier by Listeria monocytogenes. Infect Immun.
884 2007;75(2):950-7.
885 15. Bakardjiev AI, Stacy BA, Portnoy DA. Growth of Listeria monocytogenes in the guinea
886 pig placenta and role of cell-to-cell spread in fetal infection. J Infect Dis. 2005;191(11):1889-97.
887 16. Drevets DA. Dissemination of Listeria monocytogenes by infected phagocytes. Infect
888 Immun. 1999;67(7):3512-7.
889 17. Tilburgs T, Crespo AC, van der Zwan A, Rybalov B, Raj T, Stranger B, et al. Human
890 HLA-G+ extravillous trophoblasts: Immune-activating cells that interact with decidual leukocytes.
891 Proc Natl Acad Sci U S A. 2015;112(23):7219-24.
892 18. Guleria I, Pollard JW. The trophoblast is a component of the innate immune system during
893 pregnancy. Nat Med. 2000;6(5):589-93.

894 19. Zeldovich VB, Bakardjiev AI. Host Defense and Tolerance: Unique Challenges in the
895 Placenta. PLOS Pathogens. 2012;8(8):e1002804.
896 20. Robbins JR, Skrzypczynska KM, Zeldovich VB, Kapidzic M, Bakardjiev AI. Placental
897 syncytiotrophoblast constitutes a major barrier to vertical transmission of Listeria monocytogenes.
898 PLoS Pathog. 2010;6(1):e1000732.
899 21. Zeldovich VB, Clausen CH, Bradford E, Fletcher DA, Maltepe E, Robbins JR, et al.
900 Placental Syncytium Forms a Biophysical Barrier against Pathogen Invasion. PLoS Pathog.
901 2013;9(12):e1003821.
902 22. Kobe B, Kajava AV. The leucine-rich repeat as a protein recognition motif. Current
903 Opinion in Structural Biology. 2001;11(6):725-32.
904 23. Shen Y, Naujokas M, Park M, Ireton K. InlB-Dependent Internalization of Listeria Is
905 Mediated by the Met Receptor Tyrosine Kinase. Cell. 2000;103(3):501-10.
906 24. Bierne H, Sabet C, Personnic N, Cossart P. Internalins: a complex family of leucine-rich
907 repeat-containing proteins in Listeria monocytogenes. Microbes Infect. 2007;9(10):1156-66.
908 25. Anderson WF. Structural Genomics and Drug Discovery for Infectious Diseases.
909 Infectious disorders drug targets. 2009;9(5):507-17.
910 26. Kim Y, Bigelow L, Borovilos M, Dementieva I, Duggan E, Eschenfeldt W, et al. Chapter
911 3. High-throughput protein purification for x-ray crystallography and NMR. Adv Protein Chem
912 Struct Biol. 2008;75:85-105.
913 27. Otwinowski Z, Minor W. Processing of X-ray diffraction data collected in oscillation
914 mode. Methods Enzymol. 1997;276:307-26.
915 28. Murshudov GN, Skubak P, Lebedev AA, Pannu NS, Steiner RA, Nicholls RA, et al.
916 REFMAC5 for the refinement of macromolecular crystal structures. Acta crystallographica
917 Section D, Biological crystallography. 2011;67(Pt 4):355-67.
918 29. Emsley P, Cowtan K. Coot: model-building tools for molecular graphics. Acta Crystallogr
919 D Biol Crystallogr. 2004;60(Pt 12 Pt 1):2126-32.
920 30. Rizzuto GA, Kapidzic M, Gormley M, Bakardjiev AI. Human Placental and Decidual
921 Organ Cultures to Study Infections at the Maternal-fetal Interface. J Vis Exp. 2016(113).
922 31. Bakardjiev AI, Stacy BA, Fisher SJ, Portnoy DA. Listeriosis in the pregnant guinea pig: a
923 model of vertical transmission. Infect Immun. 2004;72(1):489-97.
924 32. Bastounis E, Meili R, Álvarez-González B, Francois J, del Álamo JC, Firtel RA, et al.
925 Both contractile axial and lateral traction force dynamics drive amoeboid cell motility. The
926 Journal of Cell Biology. 2014;204(6):1045-61.
927 33. Lamason RL, Bastounis E, Kafai NM, Serrano R, Del Alamo JC, Theriot JA, et al.
928 Rickettsia Sca4 Reduces Vinculin-Mediated Intercellular Tension to Promote Spread. Cell.
929 2016;167(3):670-83.e10.
930 34. Gui L, Wereley ST. A correlation-based continuous window-shift technique to reduce the
931 peak-locking effect in digital PIV image evaluation. Exp Fluids. 2002;32:506-17.
932 35. del Álamo JC, Meili R, Alonso-Latorre B, Rodríguez-Rodríguez J, Aliseda A, Firtel RA,
933 et al. Spatio-temporal analysis of eukaryotic cell motility by improved force cytometry. Proc Nat
934 Acad Sci. 2007;104(33):13343-8.
935 36. Banerjee I, Carrion K, Serrano R, Dyo J, Sasik R, Lund S, et al. Cyclic stretch of
936 embryonic cardiomyocytes increases proliferation, growth, and expression while repressing Tgf-β
937 signaling. Journal of Molecular and Cellular Cardiology. 2015;79:133-44.

938 37. Zeldovich VB, Robbins JR, Kapidzic M, Lauer P, Bakardjiev AI. Invasive extravillous
939 trophoblasts restrict intracellular growth and spread of Listeria monocytogenes. PLoS Pathog.
940 2011;7(3):e1002005.
941 38. Ortega FE, Rengarajan M, Chavez N, Radhakrishnan P, Gloerich M, Bianchini J, et al.
942 Adhesion to the host cell surface is sufficient to mediate Listeria monocytogenes entry into
943 epithelial cells. Mol Biol Cell. 2017.
944 39. Zhou X, Massol RH, Nakamura F, Chen X, Gewurz BE, Davis BM, et al. Remodeling of
945 the Intestinal Brush Border Underlies Adhesion and Virulence of an Enteric Pathogen. mBio.
946 2014;5(4):e01639-14.
947 40. Mandai K, Rikitake Y, Shimono Y, Takai Y. Afadin/AF-6 and canoe: roles in cell
948 adhesion and beyond. Prog Mol Biol Transl Sci. 2013;116:433-54.
949 41. Ikeda W, Nakanishi H, Miyoshi J, Mandai K, Ishizaki H, Tanaka M, et al. Afadin: A key
950 molecule essential for structural organization of cell-cell junctions of polarized epithelia during
951 embryogenesis. J Cell Biol. 1999;146(5):1117-32.
952 42. Zhadanov AB, Provance DW, Jr., Speer CA, Coffin JD, Goss D, Blixt JA, et al. Absence
953 of the tight junctional protein AF-6 disrupts epithelial cell-cell junctions and cell polarity during
954 mouse development. Curr Biol. 1999;9(16):880-8.
955 43. Sawyer JK, Harris NJ, Slep KC, Gaul U, Peifer M. The Drosophila afadin homologue
956 Canoe regulates linkage of the actin cytoskeleton to adherens junctions during apical constriction.
957 The Journal of Cell Biology. 2009;186(1):57-73.
958 44. Schubert WD, Urbanke C, Ziehm T, Beier V, Machner MP, Domann E, et al. Structure of
959 internalin, a major invasion protein of Listeria monocytogenes, in complex with its human
960 receptor E-cadherin. Cell. 2002;111(6):825-36.
961 45. Serra-Picamal X, Conte V, Vincent R, Anon E, Tambe DT, Bazellieres E, et al.
962 Mechanical waves during tissue expansion. Nature Physics. 2012;8:628.
963 46. Bazellières E, Conte V, Elosegui-Artola A, Serra-Picamal X, Bintanel-Morcillo M, Roca-
964 Cusachs P, et al. Control of cell–cell forces and collective cell dynamics by the intercellular
965 adhesome. Nat Cell Biol. 2015;17(4):409-20.
966 47. Rengarajan M, Hayer A, Theriot JA. Endothelial Cells Use a Formin-Dependent
967 Phagocytosis-Like Process to Internalize the Bacterium Listeria monocytogenes. PLoS Pathog.
968 2016;12(5):e1005603.
969 48. Ferrell N, Groszek J, Li L, Smith R, Butler RS, Zorman CA, et al. Basal lamina secreted
970 by MDCK cells has size- and charge-selective properties. Am J Physiol Renal Physiol.
971 2011;300(1):F86-90.
972 49. PrabhuDas M, Bonney E, Caron K, Dey S, Erlebacher A, Fazleabas A, et al. Immune
973 mechanisms at the maternal-fetal interface: perspectives and challenges. Nat Immunol. 16. United
974 States2015. p. 328-34.
975 50. Parida SK, Domann E, Rohde M, Muller S, Darji A, Hain T, et al. Internalin B is essential
976 for adhesion and mediates the invasion of Listeria monocytogenes into human endothelial cells.
977 Mol Microbiol. 1998;28(1):81-93.
978 51. Kirchner M, Higgins DE. Inhibition of ROCK activity allows InlF-mediated invasion and
979 increased virulence of Listeria monocytogenes. Mol Microbiol. 2008;68(3):749-67.
980 52. Sabet C, Lecuit M, Cabanes D, Cossart P, Bierne H. LPXTG protein InlJ, a newly
981 identified internalin involved in Listeria monocytogenes virulence. Infect Immun.
982 2005;73(10):6912-22.

983 53. Tsurumi H, Kurihara H, Miura K, Tanego A, Ohta Y, Igarashi T, et al. Afadin is localized
984 at cell–cell contact sites in mesangial cells and regulates migratory polarity. Laboratory
985 Investigation. 2015;96:49.
986 54. Gouin E, Adib-Conquy M, Balestrino D, Nahori M-A, Villiers V, Colland F, et al. The
987 Listeria monocytogenes InlC protein interferes with innate immune responses by targeting the IκB
988 kinase subunit IKKα. Proceedings of the National Academy of Sciences of the United States of
989 America. 2010;107(40):17333-8.
990 55. Rajabian T, Gavicherla B, Heisig M, Muller-Altrock S, Goebel W, Gray-Owen SD, et al.
991 The bacterial virulence factor InlC perturbs apical cell junctions and promotes cell-to-cell spread
992 of Listeria. Nat Cell Biol. 2009;11(10):1212-8.
993 56. Christensen KA, Myers JT, Swanson JA. pH-dependent regulation of lysosomal calcium
994 in macrophages. J Cell Sci. 2002;115(Pt 3):599-607.
995 57. Shaughnessy LM, Hoppe AD, Christensen KA, Swanson JA. Membrane perforations
996 inhibit lysosome fusion by altering pH and calcium in Listeria monocytogenes vacuoles. Cell
997 Microbiol. 2006;8(5):781-92.
998 58. Thai TL, Yu L, Galarza-Paez L, Wu MM, Lam HY, Bao HF, et al. The Polarized Effect of
999 Intracellular Calcium on the Renal Epithelial Sodium Channel Occurs as a Result of Subcellular
1000 Calcium Signaling Domains Maintained by Mitochondria. J Biol Chem. 2015;290(48):28805-11.
1001 59. Kiselyov K, Wang X, Shin DM, Zang W, Muallem S. Calcium signaling complexes in
1002 microdomains of polarized secretory cells. Cell Calcium. 2006;40(5-6):451-9.
1003 60. Cantero Mdel R, Cantiello HF. Calcium transport and local pool regulate polycystin-2
1004 (TRPP2) function in human syncytiotrophoblast. Biophys J. 2013;105(2):365-75.
1005 61. Saenz HL, Engel P, Stoeckli MC, Lanz C, Raddatz G, Vayssier-Taussat M, et al. Genomic
1006 analysis of Bartonella identifies type IV secretion systems as host adaptability factors. Nat Genet.
1007 2007;39(12):1469-76.
1008 62. Roux CM, Rolan HG, Santos RL, Beremand PD, Thomas TL, Adams LG, et al. Brucella
1009 requires a functional Type IV secretion system to elicit innate immune responses in mice. Cell
1010 Microbiol. 2007;9(7):1851-69.
1011 63. Coburn B, Sekirov I, Finlay BB. Type III secretion systems and disease. Clin Microbiol
1012 Rev. 2007;20(4):535-49.
1013 64. Backert S, Meyer TF. Type IV secretion systems and their effectors in bacterial
1014 pathogenesis. Curr Opin Microbiol. 2006;9(2):207-17.
1015 65. Tanaka-Okamoto M, Hori K, Ishizaki H, Itoh Y, Onishi S, Yonemura S, et al. Involvement
1016 of afadin in barrier function and homeostasis of mouse intestinal epithelia. J Cell Sci. 2011;124(Pt
1017 13):2231-40.
1018 66. Severson EA, Lee WY, Capaldo CT, Nusrat A, Parkos CA. Junctional adhesion molecule
1019 A interacts with Afadin and PDZ-GEF2 to activate Rap1A, regulate beta1 integrin levels, and
1020 enhance cell migration. Mol Biol Cell. 2009;20(7):1916-25.
1021 67. Yamamoto T, Mori T, Sawada M, Matsushima H, Ito F, Akiyama M, et al. Loss of AF-
1022 6/afadin induces cell invasion, suppresses the formation of glandular structures and might be a
1023 predictive marker of resistance to chemotherapy in endometrial cancer. BMC Cancer.
1024 2015;15:275.
1025 68. Iwasawa N, Negishi M, Oinuma I. R-Ras controls axon branching through afadin in
1026 cortical neurons. Molecular Biology of the Cell. 2012;23(14):2793-804.

1027 69. Robbins JR, Zeldovich VB, Poukchanski A, Boothroyd JC, Bakardjiev AI. Tissue barriers
1028 of the human placenta to infection with Toxoplasma gondii. Infect Immun. 2012;80(1):418-28.
1029 70. Groschwitz KR, Hogan SP. Intestinal barrier function: molecular regulation and disease
1030 pathogenesis. J Allergy Clin Immunol. 2009;124(1):3-20; quiz 1-2.
1031 71. Melton-Witt JA, Rafelski SM, Portnoy DA, Bakardjiev AI. Oral Infection with Signature-
1032 Tagged Listeria monocytogenes Reveals Organ-Specific Growth and Dissemination Routes in
1033 Guinea Pigs. Infection and Immunity. 2012;80(2):720-32.

1034

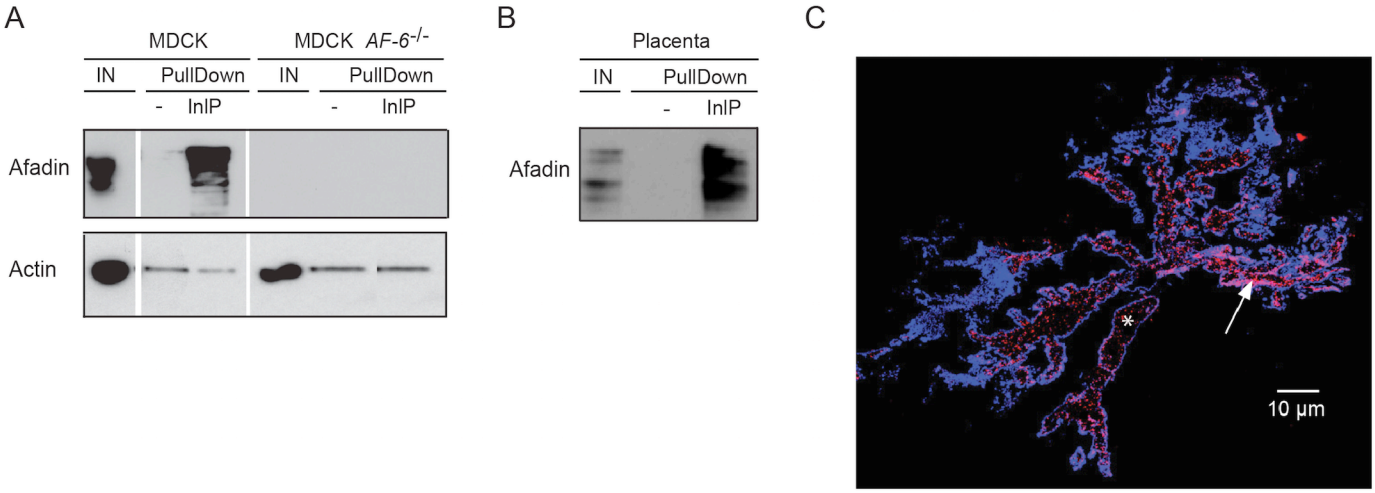
A
MDCK
MDCK AF-6-/-
IN
PullDown
IN
PullDown
-
InIP
-
InIP
Afadin
Actin
B
Placenta
IN
PullDown
-
InIP
Afadin
C
10 µm

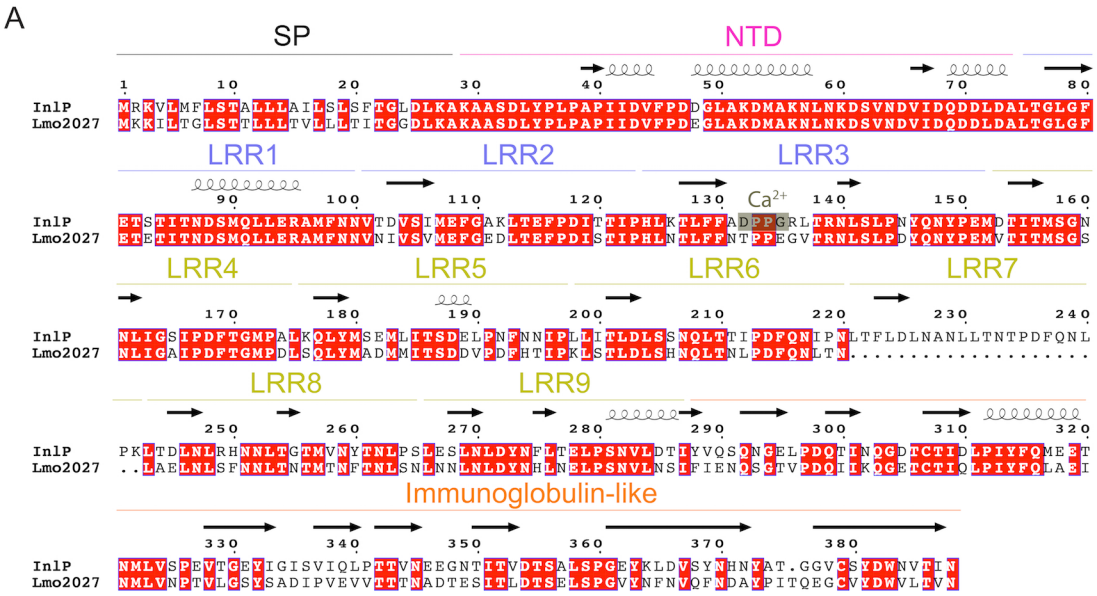
A
SP
NTD
LRR1
LRR2
LRR3
Ca2+
LRR4
LRR5
LRR6
LRR7
LRR8
LRR9
Immunoglobulin-like
InlP
Lmo2027

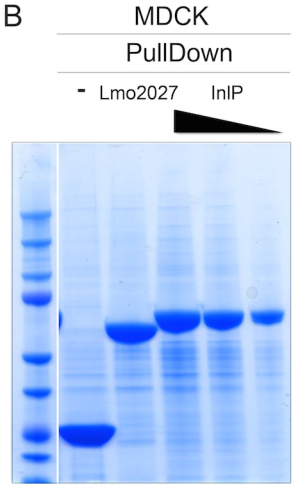
B
MDCK
PullDown
-
Lmo2027
InlP

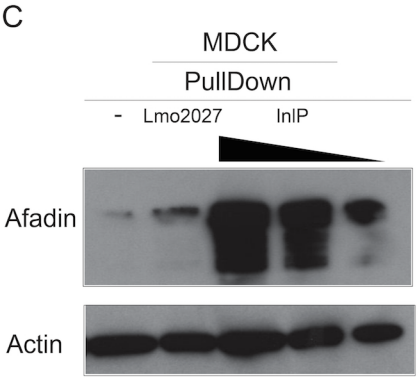
C
MDCK
PullDown
-
Lmo2027
InlP
Afadin
Actin

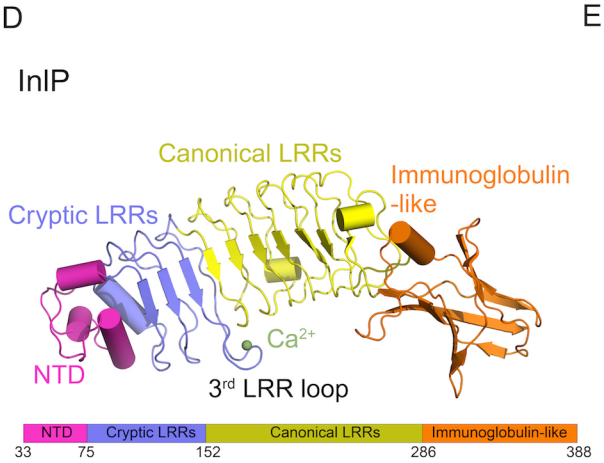
D
InlP
Canonical LRRs
Immunoglobulin -like
Cryptic LRRs
Ca2+
NTD
3rd LRR loop
NTD
Cryptic LRRs
Canonical LRRs
Immunoglobulin-like
33
75
152
286
388

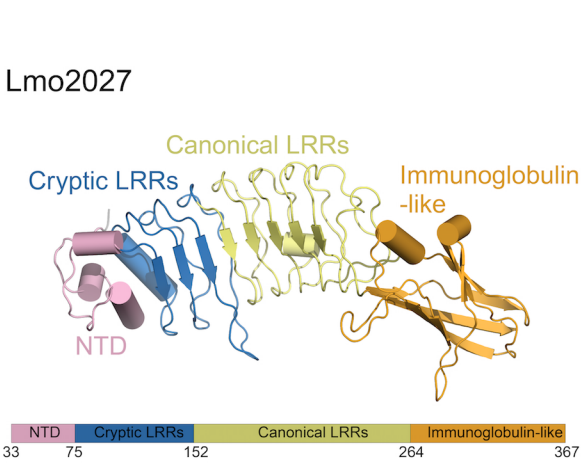
E
Lmo2027
Canonical LRRs
Cryptic LRRs
Immunoglobulin -like
NTD
NTD
Cryptic LRRs
Canonical LRRs
Immunoglobulin-like
33
75
152
264
367

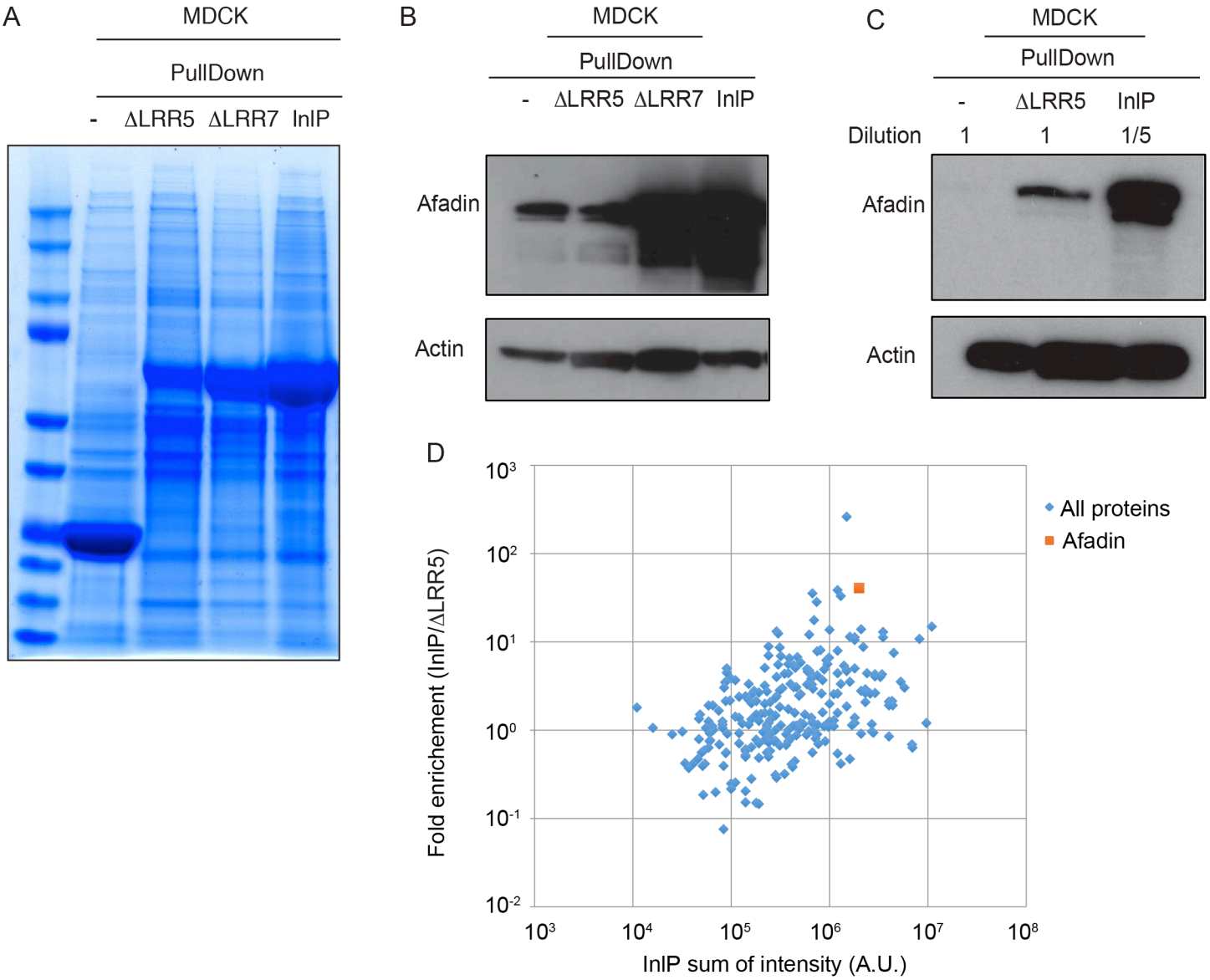
A
MDCK
PullDown
- ΔLRR5 ΔLRR7 InlP
B
MDCK
PullDown
- ΔLRR5 ΔLRR7 InlP
Afadin
Actin
C
MDCK
PullDown
- ΔLRR5 InlP
Dilution 1 1 1/5
Afadin
Actin
D
Fold enrichement (InlP/ΔLRR5)
InlP sum of intensity (A.U.)
All proteins
Afadin

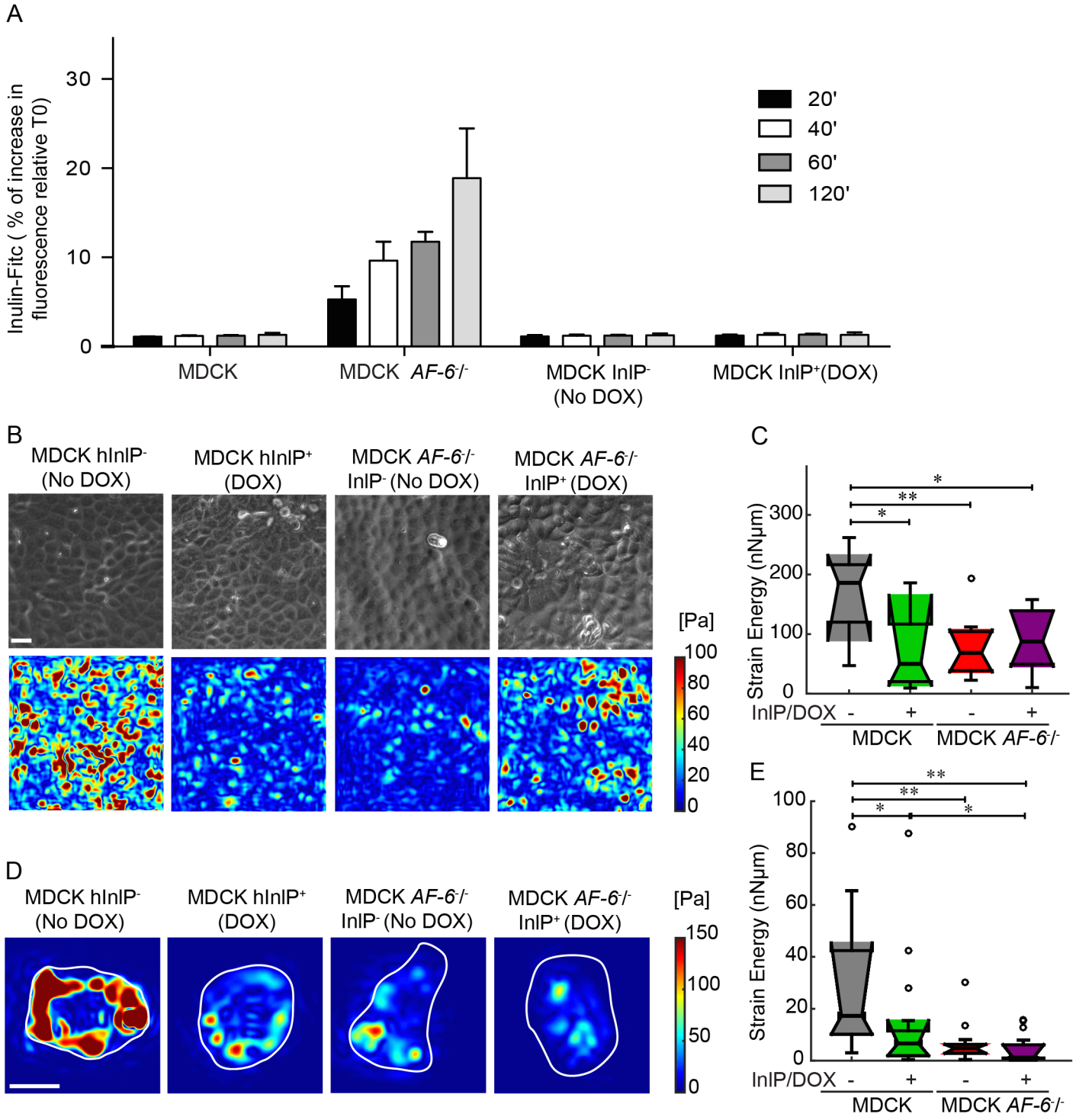
A
Inulin-Fitc (% of increase in fluorescence relative T0)
30
20
10
0
20'
40'
60'
120'
MDCK
MDCK AF-6-/-
MDCK InIP-
(No DOX)
MDCK InIP+(DOX)
B
MDCK hInIP-
(No DOX)
MDCK hInIP+
(DOX)
MDCK AF-6-/-
InIP- (No DOX)
MDCK AF-6-/-
InIP+ (DOX)
[Pa]
100
80
60
40
20
0
C
Strain Energy (nNµm)
300
200
100
0
*
**
*
InIP/DOX - + - +
MDCK
MDCK AF-6-/-
D
MDCK hInIP-
(No DOX)
MDCK hInIP+
(DOX)
MDCK AF-6-/-
InIP- (No DOX)
MDCK AF-6-/-
InIP+ (DOX)
[Pa]
150
100
50
0
E
Strain Energy (nNµm)
100
80
60
40
20
0
**
**
*
*
InIP/DOX - + - +
MDCK
MDCK AF-6-/-

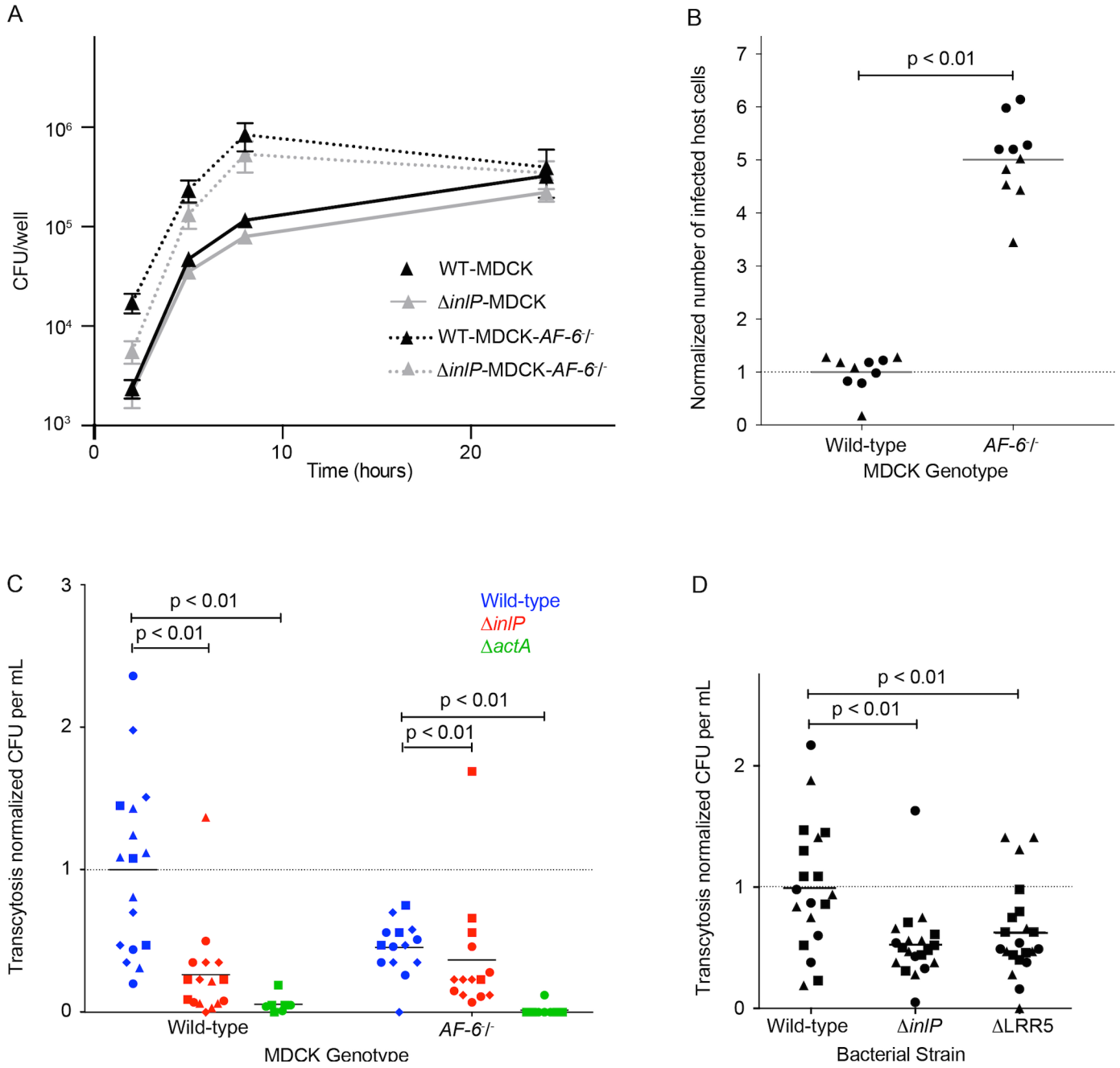
A
CFU/well
10^6
10^5
10^4
10^3
0
10
20
Time (hours)
WT-MDCK
ΔinlP-MDCK
WT-MDCK-AF-6-/-
ΔinlP-MDCK-AF-6-/-
B
Normalized number of infected host cells
p < 0.01
Wild-type
AF-6-/-
MDCK Genotype
C
Transcytosis normalized CFU per mL
p < 0.01
p < 0.01
p < 0.01
p < 0.01
Wild-type
ΔinlP
ΔactA
Wild-type
AF-6-/-
MDCK Genotype
D
Transcytosis normalized CFU per mL
p < 0.01
p < 0.01
Wild-type
ΔinlP
ΔLRR5
Bacterial Strain

Table 1. Yeast two-hybrid screening of human placenta library
Results summary listing the protein partners identified (gene name), the number of independent clones and the global PBS [a]. Ordering is performed based on global PBS and then on number of clones. Afadin is indicated in red.

Gene name	Number of independent clones	Global PBS [a]
RPS8	26	A
RBM5	14	A
TSHZ1	12	A
RPL5	9	A
AEBP1	7	A
NAB2	6	A
THAP3	6	A
NAB1	4	A
DNMT3A	5	B
SAFB	5	B
ZNF653	5	B
EXOSC3	4	B
RPL7A	4	B
AF6	3	B
FLJ22329	3	B
SP3	3	B
ZNF653	5	B
ZNF6	3	C
CDC27	2	C
EPS8L2	2	C
PHF23	2	C
ZNF283	2	C

[a]Global Predicted Biological Score (PBS). Confidence score of each interaction. A: very high confidence interaction; B: high confidence in the interaction; and C: good confidence in the interaction.

Table 2. Mass spectrometry data from pull-downs of InlP-GST.

Proteins identified with more than 10 unique peptides from human placental extract pull-downs are outlined below and ordered based on descending molecular weight. Black and blue gels correspond to sections A and B respectively (see Supplementary Figure 1). Afadin is indicated in red. Columns 3-5 correspond to pull-downs from placental extract with InlP-GST. Columns 6-7 show the corresponding total intensities from mass spectrometry data using InlP-GST and GST alone as baits to identify host binding partners in extracts from MDCK cell cultures.

		Placental extract pull-down			MDCK extract pull-down	
Gene name	**Molecular weight (kDa)**	**Unique peptides**	**Total peptides**	**Total Intensity InlP-GST**	**Total Intensity InlP-GST**	**Total Intensity GST**
AHNAK	628.70	54	67	$1.2x10^5$	$3.3x10^6$	$1.6x10^6$
DYNC1H1	532.07	39	54	$7.6x10^5$	$1.7x10^6$	$6x10^4$
COL6A3*	343.66	24	27	$2.5x10^5$	0	0
FLNA	280.56	79	124	$1.3x10^6$	$2.9x10^6$	$9.9x10^5$
FLNB	277.99	29	38	$5.7x10^5$	$6.4x10^6$	$3x10^6$
TPR*	267.29	29	39	$6.3x10^5$	0	0
MYH9	226.39	14	17	$1.2x10^5$	$4.1x10^7$	$1.2x10^7$
AF6	206.68	18	23	$5.3x10^5$	$2x10^6$	0
COL14A1*	193.51	11	12	$1.6x10^5$	0	0
CLTC	191.49	20	26	$4.0x10^5$	$9.8x10^6$	$9x10^6$
IQGAP1	189.13	25	31	$3.9x10^5$	$9.6x10^6$	$1.9x10^5$
TNKS1BP1	181.69	15	19	$1.5x10^5$	$7.9x10^4$	0
FN1*	181.23	11	14	$3.4x10^5$	0	0
KIF5B	109.62	13	15	$2.6x10^5$	$4.3x10^6$	$1.9x10^5$
ACADVL*	70.39	12	16	$1.6x10^6$	0	0
CALD1*	62.66	13	27	$3.7x10^6$	0	0
ANXA1	54.36	12	23	$1.2x10^7$	$2x10^8$	$2.5x10^7$
VIM	53.62	16	27	$5.7x10^6$	$3x10^7$	$1x10^7$
ANXA2	38.58	18	38	$2.3x10^7$	$2x10^6$	$x10^6$
ANXA5	35.91	11	14	$7.9x10^6$	$7.7x10^5$	$6.5x10^6$
GSTP1*	23.35	11	24	$3.2x10^7$	0	0

* Asterisk denotes that no peptides were identified in extracts from MDCK cell cultures.

Table 3. Crystallographic Table

Data Collection and Refinement Statistics[a]

	InlP	Lmo2027
PDB code	5HL3	5KZS
Data Collection		
Resolution range, Å	30.00-1.40 (1.42-1.40)	30.00-2.30 (2.34-2.30)
Space group	$P4_12_12$	I_4
Unit cell dimensions		
a,b,c, Å	a & b= 72.9 c = 179.5	a & b = 157.8 c = 36.3
α, β, γ, degrees	α, β, γ = 90	α, β, γ = 90
Completeness, %	99.8 (100)	98.6 (99.6)
No. reflections	180423 (9031)	20005 (1429)
Redundancy	45.6 (5.3)	6.2 (4.5)
$\langle I/\sigma(I) \rangle$	30.2 (2.6)	79.7 (2.0)
R_{merge}, %	7.9 (65.3)	9.0 (57.1)
Refinement statistics		
R-factor (R_{work}/R_{free})[b]	16.0/17.6	22.8/27.9
No. atoms		
Protein	2935	2377
Waters	828	26
Ca^{2+}	8	n/a
R.M.S. deviations		
Bond lengths, Å	0.011	0.009
Bond angles, degrees	1.51	1.47
Ramachandran analysis		
Favored regions, %	96	95
Allowed regions, %	100	99
Disallowed regions, %	0	1

[a] Highest resolution shell in parenthesis.

[b] Definition of R_{work}, R_{free}: $R=\Sigma_{hkl}\big||F_{obs}|-|F_{calc}|\big| / \Sigma_{hkl}|F_{obs}|$, where *hkl* are the reflection indices used in refinement for **R_{work}, and 5% not used in refinement for R_{free}**. F_{obs} and F_{calc} are structure factors deduced from measured intensities or calculated from the model, respectively.